Check for updates

JGR Solid Earth

RESEARCH ARTICLE
10.1029/2024JB030527

The Viscosity of Albitic Melt at High Pressures and Implications for the Mobility of Crust-Forming Magmas

Aaron Wolfgang Ashley[1], Mainak Mookherjee[1], Man Xu[2,3], Tony Yu[2], Geeth Manthilake[4], and Yanbin Wang[2]

[1]Earth Materials Laboratory, Department of Earth, Ocean and Atmospheric Sciences, Florida State University, Tallahassee, FL, USA, [2]Center for Advanced Radiation Sources, The University of Chicago, Chicago, IL, USA, [3]Shanghai Advanced Research in Physical Sciences, Center for High Pressure Science & Technology Advanced Research, Shanghai, China, [4]Laboratoire Magmas et Volcans CNRS, IRD, OPGC, Université Clermont Auvergne, Clermont-Ferrand, France

Abstract The earliest form of continental crust was produced by tonalite-trondhjemite-granodiorite (TTG) magmas. Molten albite ($NaAlSi_3O_8$) is representative of TTGs and also a major component of modern crust-forming magma. The viscosity of the melt controls the magma ascent rate and hence influences the production of new continental crust. It is well known that the viscosity (η) of albitic melt exhibits an anomalous pressure (P) dependence. However, prior results on the melt η at high-P differ significantly which limits our ability to predict the movement of crust-forming magma at depth. In this study, we more tightly constrained the P-effect on η in anhydrous albitic melt via high-P and high-temperature (T) falling sphere experiments. We limited undesirable drag effects by using small sphere-to-capsule diameter ratios (d/D) such that $d/D \leq 0.12$, and evaluated uncertainties due to such drag using a Monte Carlo approach. Our results show that melt η first decreases with P (i.e., $\partial\eta/\partial P < 0$) and then increases with continued compression ($\partial\eta/\partial P > 0$) with a well-defined η minimum (η_{min}) at ~6 GPa along a ~2,000 K isotherm. We find that the viscosity of the melt can be described by an Arrhenius formalism with an activation volume that varies with P and T. The results indicate that η of aluminosilicate magmas decrease with depth and temperature in the crust, thereby mobilizing the magmas to promote rapid volcanic eruptions. The results also suggest that TTG magmas relevant for the early Earth could pond during ascent due to the anomalous P-effect on η.

Plain Language Summary The continental crust is produced by silica-rich magma which shows a similar composition to the mineral albite. Viscosity controls the ascent rate of the magma. High-pressure experiments have shown that the viscosity of molten albite displays an anomalous pressure dependence. These are challenging experiments and the results disagree on the exact effect of pressure. In this study, we more tightly constrain the pressure dependence of the melt viscosity using high-pressure experiments. We resolve uncertainties in our measurements using a statistical approach. Our results show that the melt viscosity decreases to a minimum at about 6 GPa and 2,000 K, and then increases with continued compression. The results indicate that magma becomes less viscous with depth in the modern crust. However, magma originating from deeper or hotter conditions, such as relevant for the early Earth, may pond due to the anomalous pressure-effect on the melt viscosity.

Key Points:

- We tightly constrained the anomalous pressure effect on the viscosity of molten albite using experiments and rigorous error analysis
- Modern aluminosilicate magma is more mobile at crustal depths due to a decrease in the melt viscosity at low pressures
- Crust-forming magma in the early Earth may have ponded during ascent due to a pressure-induced minimum in the melt viscosity

Supporting Information:

Supporting Information may be found in the online version of this article.

Correspondence to:

A. W. Ashley,
awashley@fsu.edu

Citation:

Ashley, A. W., Mookherjee, M., Xu, M., Yu, T., Manthilake, G., & Wang, Y. (2025). The viscosity of albitic melt at high pressures and implications for the mobility of crust-forming magmas. *Journal of Geophysical Research: Solid Earth*, *130*, e2024JB030527. https://doi.org/10.1029/2024JB030527

Received 11 OCT 2024
Accepted 25 APR 2025

Author Contributions:

Conceptualization: Aaron Wolfgang Ashley, Mainak Mookherjee
Data curation: Aaron Wolfgang Ashley
Formal analysis: Aaron Wolfgang Ashley
Funding acquisition: Mainak Mookherjee, Yanbin Wang
Investigation: Aaron Wolfgang Ashley, Mainak Mookherjee
Methodology: Aaron Wolfgang Ashley, Mainak Mookherjee, Man Xu, Tony Yu, Geeth Manthilake, Yanbin Wang
Project administration: Mainak Mookherjee, Yanbin Wang
Resources: Mainak Mookherjee, Man Xu, Tony Yu, Geeth Manthilake, Yanbin Wang
Software: Aaron Wolfgang Ashley
Supervision: Mainak Mookherjee, Man Xu, Tony Yu, Geeth Manthilake, Yanbin Wang
Validation: Aaron Wolfgang Ashley

© 2025. American Geophysical Union. All Rights Reserved.

1. Introduction

Melt with an albite stoichiometry ($NaAlSi_3O_8$) is an analog for aluminosilicate magmas which produce new continental crust. For instance, tonalite-trondhjemite-granodiorites (TTGs) characterize the continental crust of the early Earth (Moyen & Martin, 2012). The TTGs are often dominated by quartz and feldspar mineralogy with high sodium (Na_2O) contents which are chemically close to the albite endmember in the albite ($NaAlSi_3O_8$)—anorthite ($CaAl_2Si_2O_8$)—K-feldspar ($KAlSi_3O_8$) ternary system (Laurent et al., 2024). Experiments suggest that TTG melts could be produced at ~20–150 km depths, that is, ~0.5–4 GPa (Moyen & Martin, 2012). In the present-day Earth, at conditions relevant to volcanic eruptions, albitic melts have very high viscosities (η), that is, >1,000 Pa s (Dingwell, 1987; Urbain et al., 1982). The high η is due to a highly connected polymer network defining the melt structure (Allwardt et al., 2007; Ashley Bajgain & Mookherjee, 2024; Poe et al., 1997). At the conditions relevant to producing the magma at high pressures, the connectivity of the melt structure is likely to increase. One may thus expect η to increase with depth. However, high-P experiments showed that the η of albitic melts decreases with compression up to 2 GPa, that is, ~60 km (Kushiro, 1978). The effect of pressure on the η of

21699356, 2025, 5, Downloaded from https://agupubs.onlinelibrary.wiley.com/doi/10.1029/2024JB030527 by Yanbin Wang - Argonne National Laboratory , Wiley Online Library on [03/06/2025]. See the Terms and Conditions (https://onlinelibrary.wiley.com/terms-and-conditions) on Wiley Online Library for rules of use; OA articles are governed by the applicable Creative Commons License

Visualization: Aaron Wolfgang Ashley, Mainak Mookherjee
Writing – original draft: Aaron Wolfgang Ashley, Mainak Mookherjee
Writing – review & editing: Aaron Wolfgang Ashley, Mainak Mookherjee, Man Xu, Tony Yu, Geeth Manthilake, Yanbin Wang

albite melt contrasts our expectations that polymerization is positively correlated with η of melts. Later studies also found that the pressure effect on η reverses with continued compression, that is, the viscosity decreases to a minimum (η_{min}) and then increases with continued compression. As an ascending crustal magma is likely to follow a nearly isothermal adiabat (Ashley Bajgain & Mookherjee, 2024), such an anomalous pressure effect on η could significantly affect the ascent rate of crust-forming melts. Yet, it remains unclear whether η_{min} of albitic melt occurs at ≥5 GPa or <5 GPa (Funakoshi et al., 2002; Mori et al., 2000). Both studies constrained the melt viscosity using the falling sphere method via Stokes' Law. However, these prior studies relied on significant corrections to Stokes' Law due to additional drag effects acting on the sphere. Such corrections may significantly increase the uncertainties in the measured viscosity and hence obscure the observed trends (Ashley, Mookherjee, et al., 2024).

The anomalous pressure dependence of transport properties has also been observed in the self-diffusion of oxygen in albitic melts (Poe et al., 1997). The ionic diffusivity can be used to estimate the viscosity via the Eyring equation to further constrain the pressure of η_{min}. However, the use of the Eyring equation to estimate the viscosity is limited since the formalism assumes certain ionic diffusing species, such as O, as the principal species affecting transport and estimates the "hopping distance" of the species, for example, $d_{O...O}$ (Tinker et al., 2004). First-principles molecular dynamics (FPMD) simulations also provide insights into the behavior of albitic melt at high pressures and predict the pressure of η_{min} changes with temperature (Ashley Bajgain & Mookherjee, 2024; Bajgain & Mookherjee, 2020). However, the FPMD simulations are often performed at higher temperature isotherms. Such viscosity results at high temperatures and pressures must be extrapolated to experimental conditions (Ashley Bajgain & Mookherjee, 2024).

The lack of clarity on the effect pressure has on the transport properties of albitic melt prevents us from gaining fundamental insight into the mobility of aluminosilicate magmas at high pressures. Robust constraints on the variation in transport properties of magma at crustal and mantle conditions are essential for interpreting geophysical observations related to magmatism at depth (Ashley, Manthilake, et al., 2025; Ashley, Mookherjee, et al., 2025; Pommier & Le-Trong, 2011). In this study, we conducted high-pressure falling sphere experiments in a multi-anvil press to constrain the precise pressure effect on the viscosity of albitic melts. We used white beam X-ray radiography to ensure robust constraints on the terminal velocities of the spheres (Kanzaki et al., 1987). To better constrain the effect of pressure on η and more clearly identify η_{min}, we explored higher pressures than previous experiments, that is, $P > 7$ GPa. Finally, to constrain the viscosity using the falling sphere method, we ensured robust measurements by using small sphere-to-capsule diameter ratios (d/D) which minimize undesirable drag effects (Ashley, Mookherjee, et al., 2024). We also assessed uncertainties in the corrections to Stokes' Law for such drag effects using a Monte Carlo approach. Our results allow us to examine the fundamental behavior of aluminosilicate-rich magmas which are crucial for producing continental crust.

2. Methods

We followed the experimental method outlined in a recent study (Ashley, Mookherjee, et al., 2024). The starting materials consisted of anhydrous, synthetic glasses with an albite stoichiometry ($NaAlSi_3O_8$). We synthesized the glasses by fusing Na_2CO_3, $Al(OH)_3$, and SiO_2 reagent-grade powders in a 1:2:6 molar ratio at ambient pressure in a 2,000 K furnace at the Laboratoire Magmas et Volcans at Université Clermont Auvergne, France. We crushed and re-melted the resulting glass three times to homogenize the material and remove volatiles. We confirmed that the starting glass was anhydrous using an Attenuated Total Reflectance module with a Hyperion-1000 Bruker Fourier Transform Infrared spectrometer at Florida State University (FSU) (Ashley, Mookherjee, et al., 2024). To remove any adsorbed moisture from the powders, we stored the glass powder in an oven at ≥373 K for at least 24 hr prior to the experiments.

We used spheres of rhenium less than 200 μm in diameter (Table 1) due to its high melting temperature and density in silicate melts (Ashley, Mookherjee, et al., 2024). Furthermore, rhenium is often ideal for high-pressure and -temperature melt experiments due to its relatively inert nature. Previous falling sphere studies only noted significant reactions between silicate melt and Re spheres when the melts contain high sulfur and/or iron contents, due to the chalco- and siderophilic affinity of Re (Mouser et al., 2021; Spice et al., 2015). The lack of both Fe and S in our melt composition limits the potential for such reactions. We did not observe any obvious changes to the sphere diameter or image contrast (i.e., sphere density and hence density contrast) during the experiments. The

Table 1
Summary of Experiments

Exp. no.	Load (tons)	Peak T (K)[a]	P at peak T (GPa)	d (μm)	Post-Exp. D (μm)[b]	z range (μm)[c]	Mean z (μm)[c]	$\Delta\rho$ at T (g cm^{-3})[d]	U_∞ (μm s^{-1})	η_W (Pa s)[b] Pre-Exp. D	Post-Exp. D	Prop. ± 1σ	C_W ± 1σ
T2824[e]	100	1,871	1.3 ± 0.6	127 ± 1	1,130 ± 60	65–132	90 ± 20	18.98	5.43 ± 0.09	25.6	23.6	0.7	6
T2827	120	2,028	2.5 ± 0.6	94 ± 3	1,350 ± 60	>2–152[f]	70 ± 50[f]	18.85	6.8 ± 0.1	11.8	11.6	0.6	2
T2861	160	1,945	4.1 ± 0.6	172 ± 2	1,330 ± 20	31–84	60 ± 20	18.59	45 ± 2	5.2	4.9	0.3	1
T2829	250	1,997	5.2 ± 0.5[g]	101 ± 1	1,270 ± 40	105–151	130 ± 30	18.48	27.1 ± 0.3	3.3	3.2	0.2	0.5
T2859	225	1,999	5.9 ± 0.7	145 ± 2	1,640 ± 40	46–104	70 ± 20	18.38	125 ± 5	1.36	1.37	0.06	0.3
T2828[h]	263	1,916	6.7 ± 0.7	102 ± 2	1,090 ± 40	211–312	260 ± 30	18.25	52 ± 2	1.74	1.62	0.07	0.3
T2860	275	2,077	6.9 ± 0.8	131 ± 2	1,580 ± 40	107–225	160 ± 40	18.27	24.7 ± 0.7	5.8	5.8	0.2	1
T2826	300	2,021	7.4 ± 0.8	131 ± 1	1,300 ± 60	26–84	50 ± 20	18.18	5.45 ± 0.04	25.7	24.6	0.4	5

Note. "Exp." for experiment, P for pressure, T for temperature, d for sphere diameter, D for the inner diameter of the graphite capsules, z for falling distance between sphere and capsule bottom during terminal velocity, $\Delta\rho$ for density contrast between sphere and melt, U_∞ for terminal velocity, η for viscosity, "prop." indicates propagated uncertainty by the Monte Carlo method, and C_W ± 1σ indicates the uncertainty based on the wall correction scheme (calculated by $\eta_W \times (1 - C_W)$). For clarity, the experiments are organized with increasing pressure downward. [a]Uncertainty in measured temperature is estimated to be ≤10 K. [b]We estimate D before compression (pre-Exp.) to be 1,600 μm with ±10% uncertainty. Values for D after the experiment (post-Exp.) were measured from back-scattered electron images. [c]The z range shows the minimum and maximum values for z. The mean z gives the average and standard deviation within the range. [d]Average density contrast from Monte Carlo simulations. We estimate the uncertainty in the sphere and melt densities to be ≤1% and ≤3%, respectively, using Monte Carlo simulations on the equations of state of rhenium (Ono, 2022) and albitic melt (Ashley, Mookherjee, et al., 2024). [e]Data previously reported (Ashley, Mookherjee, et al., 2024). [f]Sphere landing was blocked from view by anvil. The z value is estimated from the lowest position of the sphere prior to falling behind the anvil and is hence a minimum estimate. [g]Pressure estimated from X-ray diffraction pattern collected at the peak temperature. Diffraction patterns collected from other experiments either did not have resolvable peaks corresponding to MgO or yielded unrealistically high pressures. In such cases, the pressures at the peak temperatures were estimated from other data (Figure 1). [h]The initial load was 400 tons, but a sudden decrease in the load, that is, a "blowout," occurred upon heating to the target temperature (Figure S1 in Supporting Information S1). The temperature and load stabilized prior to the sphere fall.

spheres were produced by flash welding 25 μm thick strips of Re foil submerged under liquid nitrogen (Xie et al., 2020, 2021). The flash electric arc was applied at 100 V.

We conducted the falling sphere experiments at the GSECARS 13-ID-D beamline at the Advanced Photon Source (APS), Argonne National Laboratory, using the T-25 Kawai-type module and 1,000-ton multi-anvil press frame (Tinker et al., 2004; Wang et al., 2009) (Figure 1). The press frame has five degrees of freedom and a positioning accuracy within 0.01 mm, allowing the sample to be accurately positioned relative to the incident X-ray beam, which is fixed in space. Two separate operating modes are used for the X-rays in the experiments. The first mode is a diffraction mode in which energy-dispersive X-ray diffraction (XRD) patterns are collected to measure pressure and determine the physical state of the samples. In the diffraction mode, a set of entrance slits collimates the incident X-ray beam to a cross-section 0.1 × 0.1 mm^2 in area. A collimator and a set of diffraction slits on the diffraction side, together with the entrance slits, define a diffraction volume with the longest dimension parallel to the incident beam. The 2θ angle was fixed at 6°. The second mode is an imaging mode in which a series of radiographic images are collected to record the falling motion of the spheres. In the imaging mode, the entrance slits of ∼1.0 × 1.5 mm^2 are used so that the sample is entirely illuminated by the beam. After the X-ray beam passes through the sample, the beam is converted to visible light by fluorescence of a 200-μm thick, single-crystal of Ce-doped lutetium aluminum garnet phosphor on the downstream side of the multi-anvil press. This visible light is reflected by a 45° mirror into a video camera through an optical lens and a series of separate radiographic images are recorded (Figure 1). We used exposure times between 0.02 and 0.05 s to record the images.

We used 14/8 multi-anvil assemblies produced by the Consortium for Materials Properties Research in Earth Sciences (Leinenweber et al., 2012). We tightly packed albitic glass powder into graphite capsules with pre-compression heights and diameters of 1.8 and 1.6 mm, respectively. We placed one Re sphere into a small indentation near the top of the glass powder within each capsule and then covered the spheres with glass powder to prevent contact with the capsule. We compressed the assemblies without heating to the target loads (Table 1). Compression typically resulted in <30% decrease in the capsule diameters. We heated the assemblies using an alternating current power supply and measured the temperature using Type-C tungsten-rhenium thermocouples above the sample. Thermal gradients in the assembly may increase the temperature toward the center of the

21699356, 2025, 5, Downloaded from https://agupubs.onlinelibrary.wiley.com/doi/10.1029/2024JB030527 by Yanbin Wang - Argonne National Laboratory , Wiley Online Library on [03/06/2025]. See the Terms and Conditions (https://onlinelibrary.wiley.com/terms-and-conditions) on Wiley Online Library for rules of use; OA articles are governed by the applicable Creative Commons License

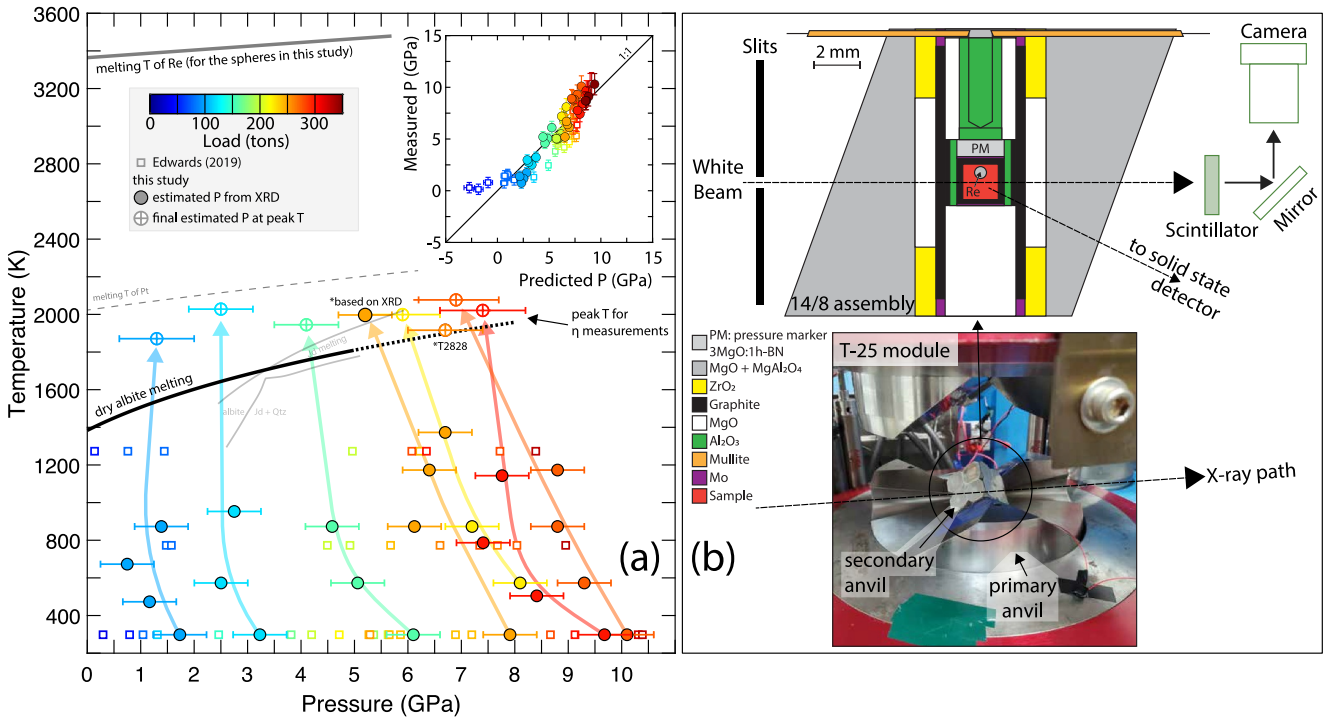

Figure 1. (a) The pressure-temperature space of the experiments in this study. Circles display experiment conditions from this study while squares show previous experiment conditions (Edwards, 2019). For this study, solid circles show pressures estimated from energy-dispersive X-ray diffraction patterns on the pressure marker. The hollow circles with "+" symbols show the final estimated pressure for experiments where the pressure could not be measured at the peak temperature (Figure S1 in Supporting Information S1). The faded arrows provide general guides for the change in pressure of each experiment. Note that only the final pressure of experiment T2828 is shown due to a blowout during heating (Table 1 and Figure S1 in Supporting Information S1). Error bars show ±1 standard deviation of uncertainty and are omitted for clarity from the previous experiments (Edwards, 2019). Lines show relevant phase boundaries for our experiments, including the anhydrous albite melting curve (Anovitz & Blencoe, 1999; Boyd & England, 1963; Shimada, 1972; Tenner et al., 2007), phase transition from albite to jadeite (Jd) ± quartz (Qtz) and their melting relations (Williams & Kennedy, 1970), and the melting curve of rhenium (Re) (Yang et al., 2012). The melting of platinum (Pt) (Anzellini et al., 2019) is also shown for reference. (b) The top shows a diagram of the experiment assembly. The bottom shows an image of the assembly in the secondary stage anvils on the T-25 module.

assembly by at least 50 K (Hernlund et al., 2006). We do not apply an correction for any such thermal gradients. A previous study showed that uncertainties in the temperature are largely negligible in Stokes' Law viscosity measurements (Ashley, Mookherjee, et al., 2024). We heated the assemblies incrementally below the melting curve of albite to allow thermal equilibration and monitor the pressure (Figure 1). After thermal equilibration, we began recording images and rapidly increased the temperature to ~2,000 K (Table 1) at a heating rate of several hundred degrees per minute. This temperature exceeds the melting curve of albite at all the explored pressures (Figure 1). We note the peak temperatures of four experiments lie below the melting curve for jadeite and quartz, which may be produced by recrystallization of albite at high pressures (Williams & Kennedy, 1970). However, we do not find obvious signs of crystallization in the recovered samples, that is, the samples were glassy after quenching. This indicates that the crystallization of jadeite ± quartz was likely too slow to affect the measurement. We allowed the spheres to settle completely, that is, either land at the bottom of the capsule or fall out of view behind one of the WC anvils, before stopping the radiographic image collection. After collecting diffraction patterns to estimate the pressure, we quenched the experiments by cutting power to the assembly.

When possible, we measured the pressures of the experiments using XRD patterns of MgO mixed with hexagonal Boron Nitride (h-BN) in a 3:1 weight ratio and the equation of state (EoS) of MgO (Tange et al., 2009). We placed compacted disks of the MgO:h-BN pressure markers directly above the sample capsules (Figure 1). We attempted to measure the pressure at the peak temperature after the spheres settled. However, the peak temperatures of the experiments promoted rapid recrystallization of the MgO in the pressure markers despite the addition of h-BN. This MgO recrystallization often obscured or distorted identifiable peaks in the diffraction patterns. Hence, the pressures could either not be determined from the patterns or were estimated to be unrealistically high. In such cases, we evaluated the pressure-temperature trends of each experiment (Figure S1 in Supporting

21699356, 2025, 5, Downloaded from https://agupubs.onlinelibrary.wiley.com/doi/10.1029/2024JB030527 by Yanbin Wang - Argonne National Laboratory , Wiley Online Library on [03/06/2025]. See the Terms and Conditions (https://onlinelibrary.wiley.com/terms-and-conditions) on Wiley Online Library for rules of use; OA articles are governed by the applicable Creative Commons License

21699356, 2025, 5, Downloaded from https://agupubs.onlinelibrary.wiley.com/doi/10.1029/2024JB030527 by Yanbin Wang - Argonne National Laboratory , Wiley Online Library on [03/06/2025]. See the Terms and Conditions (https://onlinelibrary.wiley.com/terms-and-conditions) on Wiley Online Library for rules of use; OA articles are governed by the applicable Creative Commons License

Information S1). In multi-anvil experiments, thermal relaxation of the assemblies often occurs from heating beyond ambient temperature, which produces an initial drop in the pressure. Continued heating may then yield a thermal expansion effect, which may increase and/or stabilize the pressure (Leinenweber et al., 2012). The complex interplay between the relaxation and expansion effects can yield significant uncertainties in the extrapolated pressures of our experiments (Figure S1 in Supporting Information S1).

To reduce the uncertainties in our estimated pressures, we combined our data with previous experiments using the same press and a similar assembly design (Edwards, 2019) to calibrate pressure to temperature and tonnage. The combined data set is well described by an empirical function given by $P \sim 5.3(\pm 0.3)\ln(\Gamma) - 0.6(\pm 0.2)\ln(T) - 18$ (± 2), where P is pressure (GPa), Γ is the applied load (tons), and T is temperature (K) (Figure 1). The calibration shows nice agreement with the separate pressure-temperature trends from each experiment (Figure S1 in Supporting Information S1). To note, the minimum uncertainty in our XRD-based measurements is ±0.5 GPa. The calibration alone predicts a smaller uncertainty in the extrapolated pressures. We therefore propagated the combined uncertainties to capture the additional error due to extrapolation. For most of the experiments, we used the calibration to calculate the pressure due to the overall lower uncertainties compared to individual trends (Figure S1 in Supporting Information S1). Experiments T2824 and T2829 are two exceptions. The first (T2824) was completed at a low load (100 tons), which we note is typically not well captured by the global calibration (Figure 1 *inset*). We instead take the average pressure from measurements in T2824, as this value shows better agreement with its unique pressure-temperature trends (Figure S1 in Supporting Information S1). For the other experiment, T2829, the final pressure was measured by XRD patterns from the pressure marker. This measured value is somewhat lower than predicted by the individual trends and global calibration, but the values still agree within ±95% confidence (Figure S1 in Supporting Information S1).

We used a MATLAB code to track the displacement of the spheres through time and determine their velocities (Ashley, Mookherjee, et al., 2024). We identified the terminal velocities by plateaus in the velocity versus falling distance profiles of the spheres (Figure 2). All the spheres in our experiments display terminal velocities before landing. Hence, Stokes' Law is valid and applicable in our experiments (Ashley, Mookherjee, et al., 2024). Stokes' Law defines the relationship between viscosity (η) and terminal velocity (U_∞) as

$$\eta_R = \frac{gd^2\Delta\rho}{18U_\infty} \tag{1}$$

where η_R refers to the "raw" or uncorrected η, g is the acceleration due to gravity, d is the diameter of the sphere, and $\Delta\rho$ is the density contrast between the sphere and the melt (Table 1). The densities of the rhenium sphere and the melt are estimated from the thermal equation of states of rhenium (Ono, 2022) and albitic melts (Ashley, Mookherjee, et al., 2024).

The finite volume of the capsules in high-pressure experiments introduces additional drag effects on the settling velocities of the spheres which must be corrected. There are multiple corrections available to account for such undesirable drag acting on the spheres (Brizard et al., 2005). For high pressure experiments, the most appropriate equation may be the Faxén correction (Ashley, Mookherjee, et al., 2024) which considers drag due to the walls of the capsules and inertia of the falling spheres (Faxén, 1922). The equation is given by

$$\eta_W = \eta_R C_W = \eta_R \cdot \left[1 - \frac{3}{16}\mathrm{Re}_n - \frac{d}{D} f\left(\frac{\mathrm{Re}_n/4}{d/D}\right) - 2.104\left(\frac{d}{D}\right) + 2.09\left(\frac{d}{D}\right)^3 - 0.95\left(\frac{d}{D}\right)^5\right] \tag{2}$$

where D is the inner diameter of the capsule, Re_n is the Reynolds number given by $\mathrm{Re}_n = \rho_S U_\infty d/\eta$, ρ_S is the sphere density, and $f\left(\frac{\mathrm{Re}_n/4}{d/D}\right)$ is a correction function of Re_n which can be solved semi-analytically (Ashley, Mookherjee, et al., 2024). In all our experiments, we find that $\mathrm{Re}_n << 10^{-3}$ and hence the drag due to inertia is negligible. A negligible inertia effect collapses C_W to yield $\eta_W = \eta_R \cdot [1 - 2.104\ (d/D) + 2.09\ (d/D)^3 - 0.95\ (d/D)^5]$. We use the subscript "$W$" to distinguish the viscosity calculated by Equation 2 from the uncorrected, raw viscosity, or η_R (Table 1).

We also tested other equations for Stokes' Law to evaluate the possible range in η. Drag effects due to the end of the capsule may be corrected by (a) $\eta_E = \eta_R/C_E = \eta_R/(1 + 9d/16z)$ (Lorentz, 1907). The z value may be best

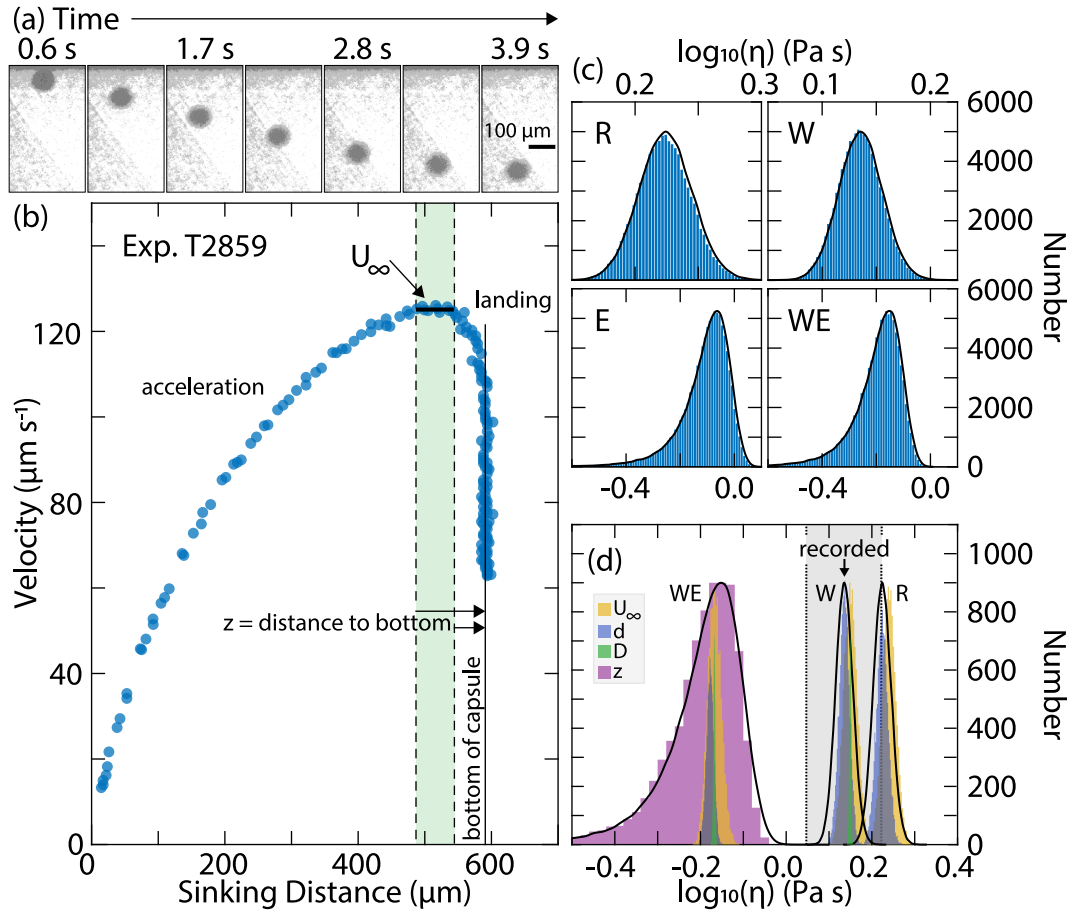

Figure 2. Results from experiment T2859 as an example. (a) Sequential radiographic images of rhenium sphere falling in anhydrous albitic melt. (b) The measured velocity of the sphere versus sinking distance. The sphere reaches terminal velocity, that is, U_∞, at the plateau indicated by an arrow and thick black line. The faded green band highlights the range over which U_∞ occurs. The landing of the sphere is identified by a rapid decrease in the velocity at a constant sinking distance (vertical line labeled "end of fall"). The z values show the distance between the sphere during U_∞ to the bottom of the capsule. (c) Histograms and probability distribution functions (PDFs) of 10^5 randomized Monte Carlo simulations for calculations of Stokes' Law. Abbreviations are "R" for uncorrected (η_R), "W" for wall-effect corrected (η_W), "E" for end-effect corrected (η_E), and "WE" for combined wall- and end-effect corrections (η_{WE}). (d) Overlain PDFs for R, W, and WE. Colored histograms show Monte Carlo simulations for one randomized variable. Outer black lines indicate the PDFs from panel (c). Abbreviations d and D are for the sphere and inner capsule diameters, respectively. The recorded mean viscosity is assumed to be η_W and is indicated by an arrow (Table 1). Dashed lines and the faded gray background show the uncertainty due to the η_W. The separate end correction results (e) are not shown in panel (d) for clarity.

described by a variable distance between the sphere and capsule end (Ashley, Mookherjee, et al., 2024; Brizard et al., 2005) (Figure 2). We recorded z as a range across which the sphere fell under terminal velocity (Table 1). There are other variations of C_E to account for drag due to the end of the capsule, including (b) $C_E = (1 + 3.3d/2z)$ (Ladenburg, 1907), and (c) $C_E = (1 + 9d/16z + (9d/16z)^2)$ (Maude, 1961). The first two variations of C_E yield comparable values of η_E while the third variation more strongly corrects the calculated viscosity (Ashley, Mookherjee, et al., 2024). However, the third C_E was also derived considering more than one sphere sinking in the melt (Maude, 1961) which does not apply to our experiments. For simplicity, we consider only the first variation of C_E (Lorentz, 1907).

The separate C_W and C_E terms have often been combined to correct the viscosity in $\eta_{WE} = \eta_R \cdot C_W/C_E$. However, combining these corrections likely overcorrects the calculated viscosity (Brizard et al., 2005). The separate corrections may instead provide a cross-comparison to ensure an accurate value of viscosity (Ashley, Mookherjee, et al., 2024). Nevertheless, we applied the combined corrections cautiously only to gauge the lowermost possible values of η for our experiments.

21699356, 2025, 5, Downloaded from https://agupubs.onlinelibrary.wiley.com/doi/10.1029/2024JB030527 by Yanbin Wang - Argonne National Laboratory , Wiley Online Library on [03/06/2025]. See the Terms and Conditions (https://onlinelibrary.wiley.com/terms-and-conditions) on Wiley Online Library for rules of use; OA articles are governed by the applicable Creative Commons License

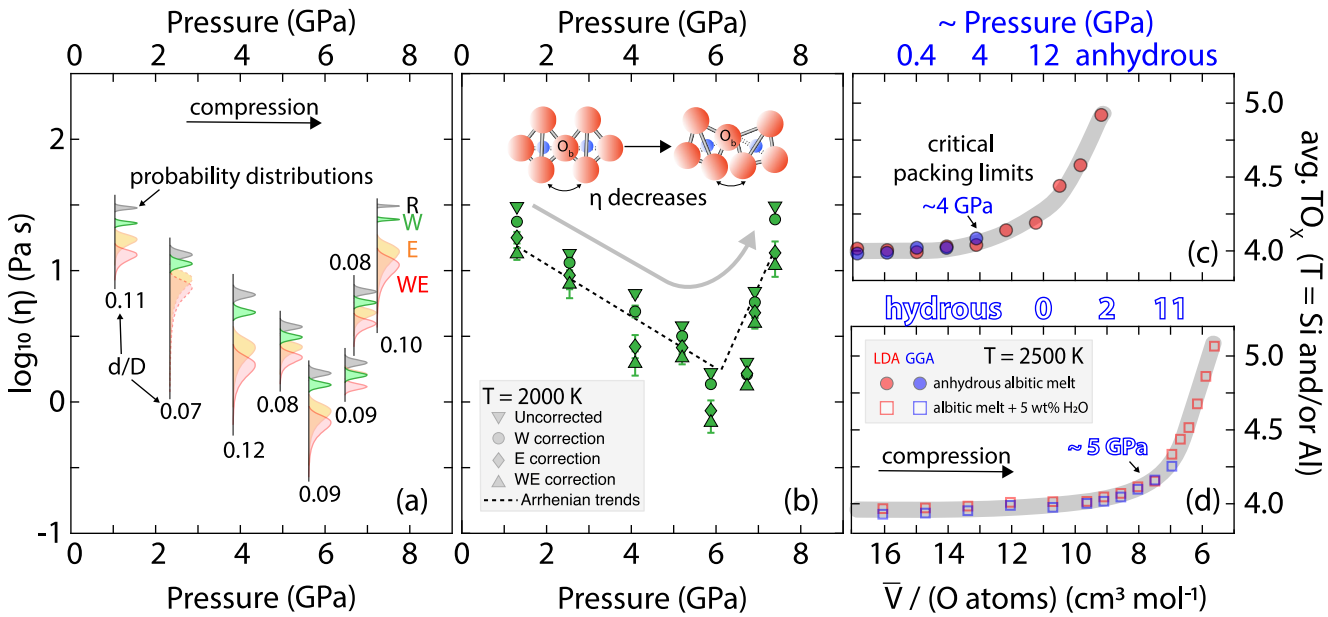

Figure 3. (a) Probability distribution functions (PDFs) from Monte Carlo results on the viscosity (η) of albitic melts from this study. Lines show the PDFs for simulations which randomly varied all parameters 10^5 times. The PDFs are color-coded for correction scheme. The abbreviations follow the description of Figure 2. The end effect corrections (E and WE) for experiment T2827 are dashed as the landing of the sphere could not be directly observed (Table 1). Numbers above and below the symbol-sets indicate the approximate d/D of the experiment after compression. (b) The average η of the melts from panel (a). Symbols indicate the type of correction applied to Stokes' Law. Error bars show ±1 standard deviation of uncertainty as estimated from Monte Carlo simulations and are typically smaller than the marker size shown. The dashed lines show two separate Arrhenian functions to describe the viscosity (fit to η_W) below and above 6 GPa (Table 2). The inset schematic diagram in panel (b) illustrates changes in the melt structure which help to decrease the viscosity with pressure. Red spheres show oxygen while blue spheres indicate Si and/or Al. The faded arrow provides a general guide for the effect of pressure on the melt structure and viscosity. (c, d) The average coordination number of network forming species, that is, TO_X where T = Si and/or Al, as a function of the molar volume of melt ($\overline{V}$) normalized by the number of oxygen atoms in the melt per mole. The panels separate first-principles molecular dynamics (FPMD) results for (c) anhydrous and (d) hydrous albitic melts, respectively (Ashley Bajgain & Mookherjee, 2024). The "LDA" and "GGA" refer to local density and generalized gradient approximations, respectively, which are types of energy exchange-correlation functionals used for FPMD simulations. The upper horizontal axes give approximate pressures based on the GGA simulations (Ashley Bajgain & Mookherjee, 2024). The $\overline{V}/(O$ atoms) ≥16 and ≥12 cm^3 mol^{-1} for the anhydrous and hydrous melts, respectively, correspond to an extensional regime in which the melts may begin to vapourize (Ashley Bajgain & Mookherjee, 2024; Kobsch & Caracas, 2020). Smaller values of $\overline{V}/(O$ atoms) correspond to a compressional regime relevant to the crust and mantle. The shaded gray areas are guides for changes in trend of the data with compression. Arrows labeled "critical packing limits" highlight inflection points where atoms can no longer be packed together, and the coordination number of TO_X increases in response (Bajgain & Mookherjee, 2020; Bajgain et al., 2019; Wang et al., 2014).

We examined statistical agreement in the variations for Stokes' Law using a Monte Carlo approach (Ashley, Mookherjee, et al., 2024). We randomly varied all input parameters for Stokes' Law and its corrections 10^5 times (Figure 2). For all parameters, we assumed normal distributions using the measured uncertainties in each parameter (Table 1). We also examined the control of each parameter on the calculated η by randomly varying one parameter while holding the others constant for 10^4 simulations. We take the minimum uncertainties in our measurements as the standard deviation of calculated viscosities from the simulations, that is, the propagated error by the Monte Carlo method (Table 1). However, we note that these propagated uncertainties from experiment parameters may underestimate the true uncertainties in viscosities due to the corrections themselves (Ashley, Mookherjee, et al., 2024). Therefore, we take the maximum possible uncertainty to be the change in calculated viscosity due to the correction, that is, % uncertainty = $100 \cdot (1 - C_W)$, where $C_W = \eta_W/\eta_R$ (Table 1 and Figure 2).

3. Results

We find that the propagated uncertainties in our values for η_W are relatively small at ≤10% at one standard deviation (Table 1). The sphere diameters, sphere sinking velocities, and capsule diameters most strongly control the uncertainties in η_W (Figure 2). For most of our experiments, the values for η_R and η_W (Equations 1 and 2) typically agree within ±95%–99% confidence based on the Monte Carlo simulations (Figure 3). The good agreement is due to a small $d/D \leq 0.12$ in our experiments (Table 1). As a result, the effect of the correction is minimized. We also note that compression of the assembly capsules does not significantly affect the calculated viscosities (Table 1).

21699356, 2025, 5, Downloaded from https://agupubs.onlinelibrary.wiley.com/doi/10.1029/2024JB030527 by Yanbin Wang - Argonne National Laboratory , Wiley Online Library on [03/06/2025]. See the Terms and Conditions (https://onlinelibrary.wiley.com/terms-and-conditions) on Wiley Online Library for rules of use; OA articles are governed by the applicable Creative Commons License

21699356, 2025, 5, Downloaded from https://agupubs.onlinelibrary.wiley.com/doi/10.1029/2024JB030527 by Yanbin Wang - Argonne National Laboratory , Wiley Online Library on [03/06/2025]. See the Terms and Conditions (https://onlinelibrary.wiley.com/terms-and-conditions) on Wiley Online Library for rules of use; OA articles are governed by the applicable Creative Commons License

Table 2
Parameters for Arrhenian Functions

Parameters	This study only V_a[a]		Exp. and FPMD $V_a(P, T)$[b]	$V_a(P, T)$ based on FPMD[c] Anhydrous[c]	~5 wt% H_2O[c]	$\partial M/\partial X_{wtH_2O}$[d]	Exp. and FPMD model adjusted to 5 wt% H_2O[e]
$\log_{10}\eta_0$(Pa s)	−3.8 ± 0.2	−10	−8.2 ± 0.6	−6.00 ± 0.09	−5.4 ± 0.2	0.10 ± 0.02	−7.7 ± 0.7
E_a (kJ mol^{-1})	200	200	410 ± 20	265 ± 5	200 ± 20	−12 ± 4	350 ± 20
V_a (cm^3 mol^{-1})	−8 ± 2	31 ± 2	–	–	–	–	–
V_1 (cm^3 mol^{-1})	–	–	−64 ± 8	−30 ± 1	−22 ± 3	1.5 ± 0.6	−57 ± 8
V_2 (×10^{-3} cm^3 mol^{-1} K^{-1})	–	–	18 ± 4	8.3 ± 0.4	7 ± 1	−0.3 ± 0.2	17 ± 4
V_3 (cm^3 mol^{-1} GPa^{-1})	–	–	−4.7 ± 0.6	0.9 ± 0.3	−0.5 ± 0.1	−0.29 ± 0.06	−6.2 ± 0.6
V_4 (×10^{-3} cm^3 mol^{-1} GPa^{-1} K^{-1})	–	–	0.3 ± 0.2	−0.30 ± 0.05	−0.04 ± 0.04	0.05 ± 0.01	0.6 ± 0.2
V_5 (cm^3 K mol^{-1} GPa^{-1})	–	–	12,530.13 ± 0.03	1,000 ± 400	2,328.56 ± 0.04	280 ± 80	13,950 ± 80

[a]The results for V_a describe two separate trends with Equation 3 to capture the anomalous pressure dependence of viscosity in only our results at ~2,000 K. These fit parameters are based on the viscosity calculated from Equation 2, that is, η_W. [b]The $V_a(P, T)$ is given by Equation 4 and describes all considered experiment and simulation results (Figure 5). [c]Model parameters taken from previous FPMD simulations (Ashley Bajgain & Mookherjee, 2024). [d]The symbol M indicates the model parameters in the first column. The X_{wtH_2O} indicates the concentration of H_2O per weight %. The values for $\partial M/\partial X_{wtH_2O}$ are calculated from the parameters based on previous FPMD simulations (Ashley Bajgain & Mookherjee, 2024), following $\partial M/\partial X_{wtH_2O} = (M_w - M_d)/(4.9\ \text{wt\%}\ H_2O)$, where M_w and M_d indicate the parameter values for the "wet" (hydrous) and "dry" (anhydrous) melts, respectively. The 4.9 wt% H_2O is taken from the precise water contents of the hydrous albitic melts in the previous work (Ashley Bajgain & Mookherjee, 2024). [e]Model parameters for $V_a(P, T)$ based on experiments and simulations, adjusted using the $\partial M/\partial X_{wtH_2O}$ values set to 5 wt% H_2O.

The calculated η_E tends to be statistically distinct from η_W and predicts lower values of viscosity (Figure 3). Combining the corrections for η_{WE} statistically agrees well with η_E. However, the propagated uncertainties for both η_E and η_{WE} are larger and more skewed than for η_W (Figure 2). This is due to a strong control of the sinking distances of the spheres, that is, z values, on the uncertainties for C_E (Ashley, Mookherjee, et al., 2024). The C_E may also be unreliable when $d/D < 0.125$ (Sutterby, 1973), as for the experiments in this study (Table 1). We further note that the Faxén correction (Equation 2) may already overcorrect Stokes' Law (Kahle et al., 2003). Therefore, calculated viscosities smaller than η_W may not be realistic (Ashley, Mookherjee, et al., 2024). Regardless of the correction to Stokes' Law, we find that the melt viscosity decreases by nearly 20-fold from ~1 to 6 GPa (Figure 3). With increasing pressure >6 GPa, the viscosity again increases and becomes comparable to η at ~1 GPa (Table 1). We note that the trend and minimum in viscosity is robust regardless of the choice in correction for Stokes' Law. Furthermore, propagated uncertainties in the calculation do not obscure the trend (Figure 3). The change in viscosity in our experiments is most likely due to the effect of pressure. We do not anticipate other influential factors, such as possible changes to the melt H_2O contents, due to the timescales needed for H_2O contamination (Text S1 in Supporting Information S1).

The effects of pressure and temperature on melt viscosity may be typically described by an Arrhenian function given by

$$\eta(P,T) = \eta_0 \cdot \exp\left(\frac{E_a + PV_a}{RT}\right) \quad (3)$$

where $\eta(P,T)$ is the viscosity at a given pressure and temperature, η_0 is the pre-exponential term, E_a is the activation energy, P is the pressure, V_a is the activation volume, R is the ideal gas law, and T is the temperature. Two separate Arrhenian functions are required to describe the observed change in trend with compression (Figure 3). The change in the pressure dependence corresponds to a change in the sign of the activation volume from negative to positive (Table 2).

4. Discussion

Our results provide key insights into the fundamental transport properties of aluminosilicate magmas. The anomalous pressure-dependence in the viscosity of albitic melts may be understood by pressure-induced changes to the atomistic scale structure of the melt. At low pressures, tetrahedrally coordinated units, that is, [TO_4] where

21699356, 2025, 5, Downloaded from https://agupubs.onlinelibrary.wiley.com/doi/10.1029/2024JB030527 by Yanbin Wang - Argonne National Laboratory , Wiley Online Library on [03/06/2025]. See the Terms and Conditions (https://onlinelibrary.wiley.com/terms-and-conditions) on Wiley Online Library for rules of use; OA articles are governed by the applicable Creative Commons License

T = Si and/or Al, are often connected via "bridging" oxygens (O_b) to form a polymerized network, that is, $[-O_3T - O_b - TO_3 -]_n$ where n describes the number of polymer units in the chain. In contrast, a "non-bridging" (O_{nb}) oxygen defines a tetrahedral corner that does not connect to another tetrahedral unit, or $[-O_3T - O_{nb}]$. At low pressures, the polymer network of an aluminosilicate-rich melt dominates the structure of the melt and hinders the diffusivity of ions, resulting in enhanced viscosity relative to aluminosilicate-poor melts (Dingwell, 1995). Previous studies have investigated the control of the melt structure on the viscosity of other aluminosilicate-rich melt compositions. The viscosity of molten jadeite ($NaAlSi_2O_6$) also decreases with compression at low pressures, based on falling sphere measurements (Suzuki et al., 2011) and FPMD simulations (Bajgain & Mookherjee, 2021; Bajgain et al., 2019). Subsequent experiments on molten jadeite based on XRD measurements showed that compression at low pressures decreases the bonding angle between the network forming polyhedral units ($\angle\overline{T - O_b - T}$), breaks some of the bridging oxygen bonds, and decreases available free space within the network (Wang et al., 2014). A decreasing $\angle\overline{T - O_b - T}$ has been also inferred from nuclear magnetic resonance (NMR) spectroscopy on aluminosilicate glasses (Kelsey et al., 2009). These structural changes help to depolymerize the melt structure and thereby decrease the melt viscosity.

With continued compression, a critical packing limit of the atoms may prevent further collapse of free space. As a result, the coordination number of Si and Al begins to increase such that TO_4 transitions to TO_5 (Wang et al., 2014). Previous NMR studies on quenched aluminosilicate melts have shown that compression may increase the Al coordination more effectively than that of Si (Allwardt, Poe, & Stebbins, 2005; Allwardt, Stebbins, et al., 2005; Allwardt et al., 2007; Lee et al., 2006, 2011; Malfait et al., 2012). The observation based on NMR spectroscopy on glasses has also been predicted by molecular dynamics simulations on melts (Ashley Bajgain & Mookherjee, 2024; Bajgain & Mookherjee, 2020; Bajgain et al., 2019; Karki et al., 2011; Kobsch & Caracas, 2020; Neilson et al., 2016). The concentration of Al in aluminosilicate melt may also help to increase the mean coordination of Al and Si together (Kelsey et al., 2009). The TO_5 polyhedral unit exchanges oxygen more readily than TO_4 which helps to enhance the diffusion of ions and thereby also decrease the melt viscosity (Schulze & Spiekermann, 2023). Previous FPMD simulations on aluminosilicate melts indicate that at relatively low pressures, where TO_4 is the dominant species, the lifetime (τ) of TO_4 is significantly greater than that of TO_5 and TO_6 species, that is, $\tau_{AlO_4} \gg \tau_{AlO_5} \gg \tau_{AlO_6}$ (Bajgain et al., 2019). At pressures where TO_5 is the dominant species, the lifetime of TO_5 is similar to that of TO_4 and TO_6 species, that is, $\tau_{AlO_4} \leq \tau_{AlO_5} \geq \tau_{AlO_6}$ (Bajgain et al., 2019). In addition to τ, the $\angle\overline{T - O_b - T}$, the fraction of O_b in the albitic melt structure also decreases with compression (Ashley Bajgain & Mookherjee, 2024; Bajgain & Mookherjee, 2020). Constraints from the previous FPMD show that the coordination of network-forming species begins to increase once atoms in the melt cannot be packed more tightly, that is, a critical packing limit is reached (Ashley Bajgain & Mookherjee, 2024; Bajgain & Mookherjee, 2020) (Figure 3). A similar effect is also observed in hydrous albitic melts. The FPMD simulations predict that continued compression of albitic melt further increases the coordination number of the network-forming species such that $TO_4 \rightarrow TO_5 \rightarrow TO_6$ (Ashley Bajgain & Mookherjee, 2024). The increasing abundance of six-fold species may involve edge-sharing of the closely packed polyhedral units (Wang et al., 2014) that could slow the diffusion of ions. As a result, the melt viscosity increases at high pressures (Figure 3).

An anomalous pressure dependence of transport properties, such as diffusion and η, is not only observed in molten albite (Bajgain & Mookherjee, 2020; Funakoshi et al., 2002; Mori et al., 2000) and jadeite (Bajgain & Mookherjee, 2021; Bajgain et al., 2019; Suzuki et al., 2011). The phenomenon has also been documented in other aluminosilicate melts such as molten anorthite ($CaAl_2Si_2O_8$) (Karki et al., 2011) and in melts with mafic to intermediate silica contents, such as basaltic (Bonechi et al., 2022; Sakamaki et al., 2013; Zhou et al., 2024) and basaltic-andesitic melts (Mouser et al., 2021) (Figure S1 in Supporting Information S1 and Figure 4). Ultramafic melts such as peridotite liquid do not typically display an obvious η_{min} along an isotherm but could instead show η_{min} along the liquidus (Xie et al., 2021) and/or along an adiabat (D. Huang et al., 2024). In the more silica-rich melts, we find that η_{min} consistently varies with temperature and silica contents (Figure 4). The presence of η_{min} in silicate melts suggests a complex variation in their mobility with depth and a possibility of ponding during ascent of a magma, which could explain low velocity zones as detected by geophysical surveys. Further, the variable pressure-effect on η with composition could play an important role in large-scale crystallization processes, such as which formed the mantle from the magma ocean (Deng et al., 2024).

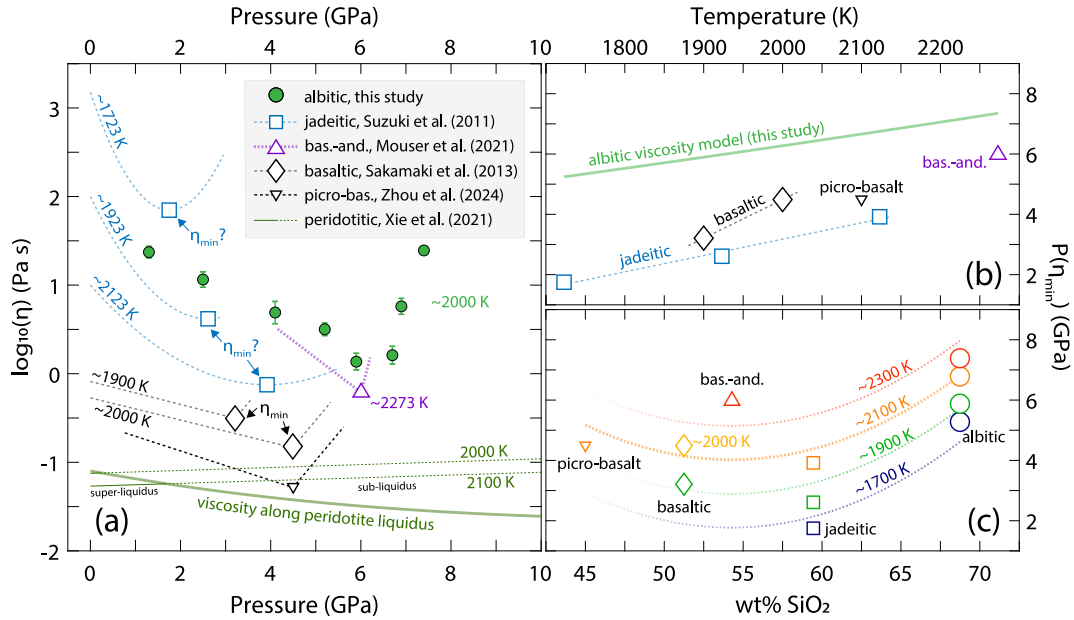

Figure 4. (a) The viscosity (η) of albitic (this study), jadeitic (Suzuki et al., 2011 and references therein), basaltic-andesitic (bas.-and.) (Mouser et al., 2021), basaltic (Sakamaki et al., 2013), picro-basaltic (Zhou et al., 2024), and peridotitic (Xie et al., 2021) melts as a function of pressure and temperature. The solid circles show data from this study using the wall correction (η_W) and the corresponding error bars indicate ±1 standard deviation of uncertainty based on the wall correction scheme (Table 1). The open symbols highlight the possible positions for η_{min} in the other melt compositions. For clarity, data from previous work is not shown (see Figure S3 in Supporting Information S1). For the jadeitic melts, empirical second-order polynomial functions are used to describe the data along each isotherm and constrain the position η_{min} by interpolation. For the bas.-and., basaltic, and picro-basaltic melts, the η_{min} are taken directly from the data. The faded solid line shows the η of peridotite melt along its liquidus as calculated from previous work (Xie et al., 2021). The thin, solid to dashed lines show the calculated peridotite melt η at super- and sub-liquidus conditions, respectively. For these isothermal η, we applied a previous Arrhenian model with $E_a = 116$ kJ mol^{-1} and $V_a = 0.63$ cm^3 mol^{-1} (Xie et al., 2021). We adjusted the previous η_0 to 70 μPa s, based on comparison to a dimensionless temperature η model which agrees well with the liquidus prediction (Xie et al., 2021). (b) The pressure of η_{min} ($P(\eta_{min})$) as a function of temperature and color-coded by melt composition for the basaltic to albitic melts. The dashed lines are linear regressions for the η_{min}. The solid line for albitic melts is calculated using Equations 3 and 4 (Table 2). (c) The P (η_{min}) as a function of SiO_2 contents and color-coded to temperature. The dashed lines are general guides for the non-linear trends suggested by the data and are calculated by $P(\eta_{min}, T, X_{SiO_2}) \sim 0.013X^2_{wtSiO_2} - 1.4X_{wtSiO_2} + 0.0056T + 32$, where X_{wtSiO_2} is the weight % of SiO_2. The circles for albitic melts are again calculated as in panel (b). In panels (b, c), the η_{min} for basaltic and jadeitic melts are taken from panel (a).

Our results help to resolve the disparity in previous studies on the viscosity of albitic melts at high pressures. Previous work has consistently observed a negative pressure-effect on the melt viscosity at <4 GPa (Funakoshi et al., 2002; Kushiro, 1978; Mori et al., 2000). We note our data show excellent agreement with other studies at ~2,000 K and these pressures (Figure 5). The most recent study (Funakoshi et al., 2002) also argued for a viscosity minimum at ~4.5 GPa at ~2,000 K, while older experiments at the same temperature did not capture such η_{min} (Mori et al., 2000). Yet, the later data (Funakoshi et al., 2002) are also at ≤5.2 GPa and hence cannot fully test the trend of the earlier work at higher pressures (Mori et al., 2000).

Crucially, the older study relied on ex situ determination of the sphere velocity after quenching (Mori et al., 2000). This ex situ tactic prevents accurate measurement of the terminal velocities, which are essential to ensuring Stokes' Law is valid (Ashley, Mookherjee, et al., 2024). Our in situ data, based on radiographic videos, show that the post-quench measurements may indeed underestimate the melt viscosity at >5.2 GPa (Figure 5). Yet, this does not explain the discrepancy between our observed η_{min} at ~6 GPa and that of previous in situ work at ~4.5 GPa (Funakoshi et al., 2002). We note that the previously constrained η_{min} depends largely on a single data point at 5.2 GPa. Furthermore, the previous work estimated very small uncertainties in their measurements, that is, ≤0.001 Pa s or ≤0.1% error (Funakoshi et al., 2002). More recent consideration of the inherent uncertainties to falling sphere experiments suggests these previous experiments may instead show ≤21% uncertainty due to corrections to Stokes' Law (Ashley, Mookherjee, et al., 2024). Hence, we find that the previous η_{min} may not be

21699356, 2025, 5, Downloaded from https://agupubs.onlinelibrary.wiley.com/doi/10.1029/2024JB030527 by Yanbin Wang - Argonne National Laboratory , Wiley Online Library on [03/06/2025]. See the Terms and Conditions (https://onlinelibrary.wiley.com/terms-and-conditions) on Wiley Online Library for rules of use; OA articles are governed by the applicable Creative Commons License

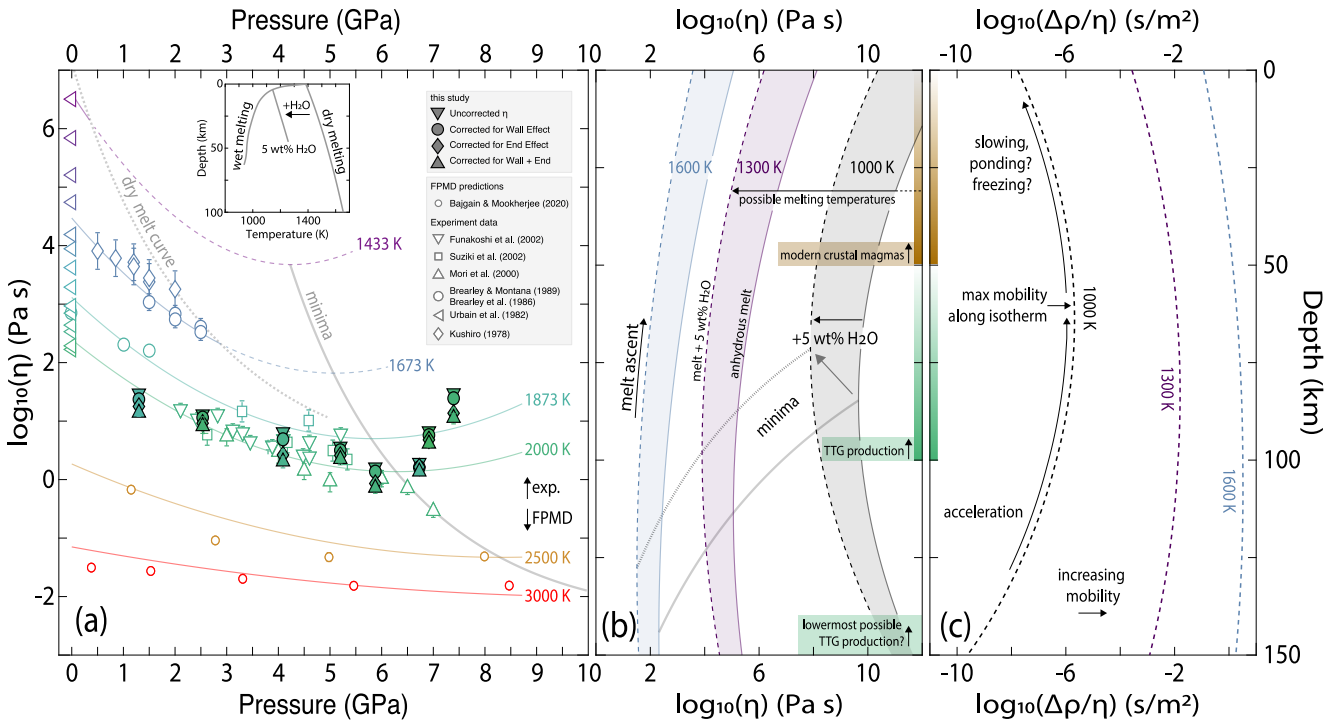

Figure 5. The viscosity of albitic melts (η) as a function of pressure and temperature based on experiments ("exp.") (Brearley & Montana, 1989; Brearley et al., 1986; Funakoshi et al., 2002; Kushiro, 1978; Mori et al., 2000; Suzuki et al., 2002; Urbain et al., 1982) and first-principles molecular dynamics simulations (Ashley Bajgain & Mookherjee, 2024; Bajgain & Mookherjee, 2020). Data above 10 GPa are not shown for clarity. Hollow symbols are values from previous work. Solid symbols are data from this study (see description in Figure 3). The solid lines show models using Equations 3 and 4 (Table 2). The faded gray line highlights η_{min} for reference. The stippled line labeled "dry melt curve" displays the η calculated along the liquidus of albite (Boyd & England, 1963; Makhluf et al., 2020; Tenner et al., 2007) (see inset). Error bars show ±1 standard deviation of uncertainty. The uncertainties for previous experiments are estimated from the reported corrections for Stokes' Law (Ashley, Mookherjee, et al., 2024). All symbols and isothermal models are color-coded by temperature. (b) The η of albitic melt with 0 and 5 wt% H_2O as a function of depth and temperature using Equations 3 and 4 (Table 2). We assume 1 GPa for every 30 km depth. Faded gray lines highlight the predicted η_{min}. The lower depth for producing modern aluminosilicate magma is ~50 km (Collins et al., 2020; W.-L. Huang & Wyllie, 1975; Skjerlie & Johnston, 1993). The lowermost boundaries for tonalite-trondhjemite-granodiorite production lie at 100–150 km (Laurent et al., 2024; Moyen & Martin, 2012). (c) The mobility ($\Delta\rho/\eta$) of the hydrous melts along several isotherms. We assume the ρ of solid albite along an Archean geothermal gradient (Figures S1 and S2 in Supporting Information S1).

robustly defined. Our work extends on these previous efforts by providing more in situ data at >5.2 GPa. The additional data more clearly resolve the effect of pressure on the melt viscosity and hence the pressure of η_{min} (Figure 5).

Notably, these experiments are several hundred degrees hotter than temperatures expected for geologically realistic production or storage of aluminosilicate magmas (Collins et al., 2020; W.-L. Huang & Wyllie, 1975; Moyen et al., 2021; Skjerlie & Johnston, 1993). We evaluated the melt viscosity across a range of pressures and temperatures relevant to subduction zones and the deep Earth (Figure 5). We also examined the viscosity at more extreme conditions (>2,000 K) to better understand the controls of pressure and temperature. Our results agree well with previous experiments at ≤2,000 K and FPMD simulations at higher temperatures (Figure 5). We note that the FPMD simulations predict η_{min} at >6 GPa for ≥2,500 K. This suggests that the anomalous pressure effect on viscosity is also dependent on temperature.

We find that all the experiment data (Brearley & Montana, 1989; Brearley et al., 1986; Funakoshi et al., 2002; Kushiro, 1978; Mori et al., 2000; Suzuki et al., 2002; Urbain et al., 1982; this study) and FPMD predictions (Ashley Bajgain & Mookherjee, 2024; Bajgain et al., 2022) at <4,000 K are well described by allowing the activation volume in Equation 3 to vary with pressure and temperature, or $V_a(P, T)$ (Figure 5). The function is given by

$$V_a(P,T) = (V_1 + V_2T) + P\left(V_3 + V_4T + \frac{V_5}{T}\right) \quad (4)$$

21699356, 2025, 5, Downloaded from https://agupubs.onlinelibrary.wiley.com/doi/10.1029/2024JB030527 by Yanbin Wang - Argonne National Laboratory , Wiley Online Library on [03/06/2025]. See the Terms and Conditions (https://onlinelibrary.wiley.com/terms-and-conditions) on Wiley Online Library for rules of use; OA articles are governed by the applicable Creative Commons License

21699356, 2025, 5, Downloaded from https://agupubs.onlinelibrary.wiley.com/doi/10.1029/2024JB030527 by Yanbin Wang - Argonne National Laboratory , Wiley Online Library on [03/06/2025]. See the Terms and Conditions (https://onlinelibrary.wiley.com/terms-and-conditions) on Wiley Online Library for rules of use; OA articles are governed by the applicable Creative Commons License

where V_1 to V_5 are empirical terms to capture the pressure and/or temperature effects on V_a (Table 2). We note that this model predicts η_{min} at 6 ± 1 GPa and ~2,000 K.

At temperatures below 2,000 K, the model predicts that the pressure of η_{min} shifts by roughly 0.2–0.4 GPa per 100 K (Figures 4 and 5). This suggests that η_{min} may occur around 2.5 GPa by 1,000 K. Such pressures are relevant for incipient melting in subduction zones (Syracuse et al., 2010). However, the necessary temperature for this pressure of η_{min} is at least a couple hundred degrees cooler than typical for such melting. We also note that the melting curve for source rocks increases dramatically with compression. For instance, the melting temperature of anhydrous albite may be ~1,650 K by 2.5 GPa (Boyd & England, 1963; Makhluf et al., 2020; Tenner et al., 2007) (Figure 1). To better examine the pressure and temperature conditions of η_{min}, we calculated the melt viscosity (Equations 3 and 4) along the melting curve of albite (Figure 5). The viscosity along the melting curve agrees well with the values determined at the maximum pressures explored by previous experiments (Brearley & Montana, 1989; Brearley et al., 1986; Funakoshi et al., 2002; Kushiro, 1978; Mori et al., 2000; Suzuki et al., 2002; Urbain et al., 1982). Considering the viscosity along an isotherm shows that the pressures required to produce η_{min} should typically stabilize solid jadeite + quartz (Figure 5).

Crucially, it is important to recognize that this study constrains the pressure and temperature effects on the viscosity of anhydrous melts. However, realistic magmas in subduction zones commonly contain several weight percent H_2O. The presence of H_2O will significantly lower the melting temperatures of source rocks by several hundred degrees (Makhluf et al., 2020) (Figure 5) and is well associated with the origin of continental crust (Campbell & Taylor, 1983). Investigating the combined pressure, temperature, and water effects on the melt viscosity is technically challenging due to the fast diffusion kinetics of hydrogen (Ashley Bajgain & Mookherjee, 2024) in silicate melts and thus the possibility of rapid escape of hydrogen during the timescale of the experiments. It is well known that dissolved H_2O in the melt dramatically lowers the melt viscosity even at high pressures (Ardia et al., 2008; Dingwell, 1987; Holtz et al., 1999; Poe et al., 2006; Schulze et al., 1996). However, these earlier experimental studies on hydrous magmas were conducted at relatively low pressures (≤2.5 GPa) and temperatures (≤1,823 K) and did not document η_{min}. Complementary FPMD simulations have documented η_{min} in hydrous aluminosilicate magmas with compression (Ashley Bajgain & Mookherjee, 2024; Bajgain et al., 2019). The combined effects of pressure, temperature, and water could shift η_{min} to conditions relevant to subduction zones or the deep crust. To further investigate the effect of water on the η and η_{min} of aluminosilicate magma at high pressures, we combine experimental results from this study and $\partial\eta/\partial X_{H_2O}$ from FPMD simulations which investigated albitic melts with ~5 wt% H_2O (Ashley Bajgain & Mookherjee, 2024; Table 2). We find that the melt viscosity should dramatically decrease with H_2O at conditions relevant to magma production (Figure 5). Our models also predict that the conditions which may produce η_{min} move upward in depth by ~3 km per wt% H_2O (Figure 5). Hence, the combined effects of H_2O on crustal melting temperatures and the viscosity of the resulting melts likely enhance the potential for ascending aluminosilicate magmas to encounter η_{min}.

We further evaluated the potential for ponding of magma via the melt mobility, that is, the contrast in density of a melt with a host matrix ($\Delta\rho = \rho_{matrix} - \rho_{melt}$) to the melt viscosity, or $\Delta\rho/\eta$ (Figure 5). For magma ascending in the early Earth, we used an EoS for crystalline albite (Benusa et al., 2005; Stewart & Limbach, 1967) as a proxy for the crustal rock matrix. We also assumed that the matrix follows an Archean geothermal gradient (Moyen & Martin, 2012) (Figure S4 in Supporting Information S1). We note the exact mineralogical composition of the host rock will influence its density (Figure S5 in Supporting Information S1). We calculate the melt ρ using the EoS for anhydrous albitic melts (Ashley, Mookherjee, et al., 2024) with the parameters adjusted to 5 wt% H_2O based on FPMD (Ashley Bajgain & Mookherjee, 2024) (Table S1 in Supporting Information S1). The anhydrous albitic melt displays a density crossover with the host matrix ($\rho_{melt} = \rho_{matrix}$) due to the higher compressibility of melt compared to its solid counterpart (Bajgain & Mookherjee, 2020; Jing & Karato, 2011; Mookherjee et al., 2016). The neutral buoyancy would enable ponding of the magma (Figure S5 in Supporting Information S1). However, adding H_2O to the melt significantly lowers the melt density and helps to prevent the density crossover at conditions relevant to the crustal melting (Figure S5 in Supporting Information S1). This yields a positive $\Delta\rho$ ($\rho_{melt} < \rho_{matrix}$) at lithospheric conditions which promotes the ascent of the magma. Yet, the $\Delta\rho$ is also typically ≤0.8 g cm^{-3}. In contrast, the change in η with depth can span orders of magnitude along an isotherm and hence dominates the trend in mobility (Figure 5). The η_{min} yields a maximum in the calculated mobility. Hence, ascending melts may accelerate to the depth of the maximum and begin to slow with continued ascent. As η

21699356, 2025, 5, Downloaded from https://agupubs.onlinelibrary.wiley.com/doi/10.1029/2024JB030527 by Yanbin Wang - Argonne National Laboratory , Wiley Online Library on [03/06/2025]. See the Terms and Conditions (https://onlinelibrary.wiley.com/terms-and-conditions) on Wiley Online Library for rules of use; OA articles are governed by the applicable Creative Commons License

increases with ascent beyond η_{min}, the slowing melt may pond or ultimately freeze (Stolper et al., 1981). Notably, silicate melts in nature are produced by partial melting and modified by reactive transport, both of which will also influence the host matrix. Corresponding changes to the melt and host rock composition will affect $\Delta\rho/\eta$ but likely also the conditions of η_{min} (Figure 4), which will further influence the depths for potential ponding. Notably, the diffusion of network-forming ions also often shows opposite pressure-trends to the viscosity (Ashley Bajgain & Mookherjee, 2024; Poe et al., 1997). The enhanced diffusivity would likely promote crystallization and/or chemical partitioning (Mollo & Hammer, 2017), which may influence geochemical and petrologic interpretation of exhumed rock.

Our results highlight the importance of understanding the effect of pressure on the viscosity of aluminosilicate magma. At the surface, aluminosilicate-rich melt tends to be extremely viscous (>1,000 Pa s) (Dingwell, 1995) due to the high degree of polymerization in the melt structure by Si and Al. We would expect such high viscosity to make the magma very sluggish before injection into magma chambers or eruption onto the surface at volcanoes. Yet very rapid volcanic eruption of aluminosilicate-rich lava, with little forewarning activity, has shown the opposite case in which the magma is significantly more mobile than expected (Castro & Dingwell, 2009). Previous FPMD studies, which examined the viscosity of aluminosilicate magma at depth in the crust, found that the decrease in melt viscosity with depth helps to mobilize the magma in such eruptions (Ashley Bajgain & Mookherjee, 2024). Our experiment results confirm that the effect of pressure on the melt viscosity steepens at cooler temperatures (Figure 5). The viscosity of magma produced or stored at ≤50 km depth (∼1.7 GPa) and <1,400 K, as typical for modern magma (Collins et al., 2020; W.-L. Huang & Wyllie, 1975; Skjerlie & Johnston, 1993) and perhaps ancient TTG melts (Laurent et al., 2024), may be an order of magnitude lower at depth compared to the surface. Hence, the magma will be significantly more mobile close to its source. Our results also shed insight into the mobilization of aluminosilicate magma originating from deeper and/or hotter conditions within the Earth, as is relevant for subduction zones or perhaps TTG magma in the early Earth (Laurent et al., 2024; Moyen & Martin, 2012). Under such conditions, the changing pressure effect on viscosity could promote slowing or ponding of ascending magma (Figure 5). Our results indicate it may be crucial to consider the anomalous pressure-dependence on silicate melt viscosity to fully evaluate magmatic processes at depth.

5. Conclusions

Our study expands on previous efforts to constrain the viscosity of anhydrous albitic melt at high pressures and temperatures. We resolve disagreements in previous studies by carefully evaluating the inherent uncertainties in falling sphere experiments and exploring a greater pressure range than previous work. Regardless of the type of correction for drag acting on falling sphere, we find robust and clear evidence for a changing pressure-effect on the melt viscosity. Compression acts to first decrease and then increase the viscosity, which yields a viscosity minimum (η_{min}) at ∼6 GPa and ∼2,000 K. The anomalous pressure effect is most likely due to multiple changes in the atomistic-scale structure of the melt, including decreasing bond angles, breaking of the network forming bonds, and increases in the packing and coordination numbers of network-forming species, namely silicon and aluminum. We find that the viscosity of albitic melt across a wide range of temperatures and pressures can be well described by a modified Arrhenius function (Equations 3 and 4, Table 2). We further extend this function to explore the effect of H_2O on the melt viscosity using constraints from previous studies. Our results indicate that aluminosilicate-rich magma in the modern crust will become less viscous, and hence more mobile, with depth. The enhanced mobility should promote extraction of the melt from its source at depth. However, magma originating from deeper or hotter conditions, such as may be relevant for crust-forming magmas in the early Earth, may also encounter viscosity minima during ascent. Such minima may promote ponding and potential freezing of the magma.

Conflict of Interest

The authors declare no conflicts of interest relevant to this study.

Data Availability Statement

All final experiment data and model parameters are provided in the main tables or Supporting Information S1. Image sequence stacks and Monte Carlo simulation files are available in a Zenodo repository (Ashley, Mookherjee, et al., 2025).

Acknowledgments
A. W. A. acknowledges the Buie, DeVore, and Watkins Fund from the Department of Earth, Ocean and Atmospheric Sciences, Florida State University. M. M. acknowledges the National Science Foundation Grant (EAR-2246802) for funding this research. A. W. A. and M. M. also acknowledge the Extreme Science and Engineering Discovery (XSEDE) and Advanced Cyberinfrastructure Coordination Ecosystem: Services and Support (ACCESS) supercomputing facilities (TG-GEO170003) and the Research Computing Center (RCC) at Florida State University (FSU) for computing resources for the FPMD simulations. M. X. acknowledges funding support from Shanghai Pujiang Program (24PJA095). G. M. acknowledges funding and resources supported by INSU and the LabEx ClerVolc (contribution number 672), which were used to synthesize the spheres and starting albitic glass. Y. W. acknowledges NSF support via EAR-2246803. The experiments were performed at GeoSoilEnviroCARS (The University of Chicago, Sector 13), Advanced Photon Source (APS), Argonne National Laboratory. GeoSoilEnviroCARS is supported by the National Science Foundation—Earth Sciences via SEES: Synchrotron Earth and Environmental Science (EAR-2223273). This research used resources of the Advanced Photon Source, a U.S. Department of Energy (DOE) Office of Science User Facility, operated for the DOE Office of Science by Argonne National Laboratory under Contract DE-AC02-06CH11357.

References

Allwardt, J. R., Poe, B. T., & Stebbins, J. F. (2005). The effect of fictive temperature on Al coordination in high-pressure (10 GPa) sodium aluminosilicate glasses. *American Mineralogist*, *90*(8–9), 1453–1457. https://doi.org/10.2138/am.2005.1736

Allwardt, J. R., Stebbins, J. F., Schmidt, B. C., Frost, D. J., Withers, A. C., & Hirschmann, M. M. (2005). Aluminum coordination and the densification of high-pressure aluminosilicate glasses. *American Mineralogist*, *90*(7), 1218–1222. https://doi.org/10.2138/am.2005.1836

Allwardt, J. R., Stebbins, J. F., Terasaki, H., Du, L. S., Frost, D. J., Withers, A. C., et al. (2007). Effect of structural transitions on properties of high-pressure silicate melts: 27 Al NMR, glass densities, and melt viscosities. *American Mineralogist*, *92*(7), 1093–1104. https://doi.org/10.2138/am.2007.2530

Anovitz, L. M., & Blencoe, J. G. (1999). Dry melting of high albite. *American Mineralogist*, *84*(11–12), 1830–1842. https://doi.org/10.2138/am-1999-11-1210

Anzellini, S., Monteseguro, V., Bandiello, E., Dewaele, A., Burakovsky, L., & Errandonea, D. (2019). In situ characterization of the high pressure – High temperature melting curve of platinum. *Scientific Reports*, *9*, 1–10. https://doi.org/10.1038/s41598-019-49676-y

Ardia, P., Giordano, D., & Schmidt, M. W. (2008). A model for the viscosity of rhyolite as a function of H_2O-content and pressure: A calibration based on centrifuge piston cylinder experiments. *Geochimica et Cosmochimica Acta*, *72*(24), 6103–6123. https://doi.org/10.1016/j.gca.2008.08.025

Ashley, A. W., Bajgain, S., & Mookherjee, M. (2024). Mobility of magmas within the Earth: Insights from the elasticity and transport properties of hydrous albitic melts. *Geochemistry, Geophysics, Geosystems*, *25*(6), e2024GC011510. https://doi.org/10.1029/2024gc011510

Ashley, A. W., Manthilake, G., Schiavi, F., & Mookherjee, M. (2025). Insights into the chemical evolution of sub-arc magmas from the high-pressure electrical conductivity of basaltic and andesitic magmas. *Geology*. https://doi.org/10.1130/G52545.1

Ashley, A. W., Mookherjee, M., Xu, M., Yu, T., Manthilake, G., & Wang, Y. (2024). Viscosity measurements at high pressures: A critical appraisal of corrections to Stokes' law. *Journal of Geophysical Research: Solid Earth*, *129*(5), e2023JB028489. https://doi.org/10.1029/2023jb028489

Ashley, A. W., Mookherjee, M., Xu, M., Yu, T., Manthilake, G., & Wang, Y. (2025). The viscosity of albitic melt at high pressures and implications for the mobility of crust-forming magmas [Dataset]. *Zenodo*. https://doi.org/10.5281/zenodo.15066705

Bajgain, S. K., Ashley, A. W., Mookherjee, M., Ghosh, D. B., & Karki, B. B. (2022). Insights into magma ocean dynamics from the transport properties of basaltic melt. *Nature Communications*, *13*(1), 7590. https://doi.org/10.1038/s41467-022-35171-y

Bajgain, S. K., & Mookherjee, M. (2020). Structure and properties of albite melt at high pressures. *ACS Earth and Space Chemistry*, *4*, 1–13. https://doi.org/10.1021/acsearthspacechem.9b00187

Bajgain, S. K., & Mookherjee, M. (2021). Carbon bearing aluminosilicate melt at high pressure. *Geochimica et Cosmochimica Acta*, *312*, 106–123. https://doi.org/10.1016/j.gca.2021.07.039

Bajgain, S. K., Peng, Y., Mookherjee, M., Jing, Z., & Solomon, M. (2019). Properties of hydrous aluminosilicate melt at high pressures. *ACS Earth and Space Chemistry*, *3*, 390–402. https://doi.org/10.1021/acsearthspacechem.8b00157

Benusa, M. D., Angel, R. J., & Ross, N. L. (2005). Compression of albite, $NaAlSi_3O_8$. *American Mineralogist*, *90*(7), 1115–1120. https://doi.org/10.2138/am.2005.1805

Bonechi, B., Stagno, V., Kono, Y., Hrubiak, R., Ziberna, L., Andreozzi, G. B., et al. (2022). Experimental measurements of the viscosity and melt structure of alkali basalts at high pressure and temperature. *Scientific Reports*, *12*(1), 2599. https://doi.org/10.1038/s41598-022-06551-7

Boyd, F. R., & England, J. L. (1963). Effect of pressure on the melting of diopside, $CaMgSi_2O_6$, and albite, $NaAlSi_3O_8$, in the range up to 50 kilobars. *Journal of Geophysical Research*, *68*(1), 311–323. https://doi.org/10.1029/jz068i001p00311

Brearley, M., Dickinson, J. E., & Scarfe, C. M. (1986). Pressure dependence of melt viscosities on the join diopside-albite. *Geochimica et Cosmochimica*, *50*(12), 2563–2570. https://doi.org/10.1016/0016-7037(86)90210-3

Brearley, M., & Montana, A. (1989). The effect of CO_2 on the viscosity of silicate liquids at high pressure. *Geochimica et Cosmochimica Acta*, *53*(10), 2609–2616. https://doi.org/10.1016/0016-7037(89)90132-4

Brizard, M., Megharfi, M., Mahé, E., & Verdier, C. (2005). Design of a high precision falling-ball viscometer. *Review of Scientific Instruments*, *76*(2), 025109. https://doi.org/10.1063/1.1851471

Campbell, I. H., & Taylor, S. R. (1983). No water, no granites - No oceans, no continents. *Geophysical Research Letters*, *10*(11), 1061–1064. https://doi.org/10.1029/gl010i011p01061

Castro, J. M., & Dingwell, D. B. (2009). Rapid ascent of rhyolitic magma at Chaitén volcano, Chile. *Nature*, *461*(7265), 780–783. https://doi.org/10.1038/nature08458

Collins, W. J., Murphy, J. B., Johnson, T. E., & Huang, H. Q. (2020). Critical role of water in the formation of continental crust. *Nature Geoscience*, *13*(5), 331–338. https://doi.org/10.1038/s41561-020-0573-6

Deng, J., Hu, J., Shi, Y., Lee, J., Niu, H., & Stixrude, L. (2024). Bridgmanite megacrysts drive segregation of the terrestrial magma ocean. *Preprint under review at Nature Portfolio*. https://doi.org/10.21203/rs.3.rs-3108549/v1

Dingwell, D. B. (1987). Melt viscosities in the system $NaAlSi_3O_8$-H_2O-F_2O. *Magmatic Processes: Physicochemical Principles*, *1*, 423–433.

Dingwell, D. B. (1995). Viscosity and anelasticity of melts. In *Mineral physics and crystallography: A handbook of physical constraints* (pp. 209–216).

Edwards, P. M. (2019). *Viscosity of iron-rich silicate melts by falling sphere viscometry at high pressure: Implications for the mobility of pyroxenitic melts in the mantle*. University of California.

Faxén, H. (1922). Der Widerstand gegen die Bewegung einer starren Kugel in einer zahen Flussigkeit, die zwischen zwei parallelen ebenen Wanden eingeschlossen is. *Annalen der Physik*, *373*(10), 89–119. https://doi.org/10.1002/andp.19223731003

Funakoshi, K. I., Suzuki, A., & Terasaki, H. (2002). In situ viscosity measurements of albite melt under high pressure. *Journal of Physics: Condensed Matter*, *14*(44), 11343–11347. https://doi.org/10.1088/0953-8984/14/44/479

Hernlund, J., Leinenweber, K., Locke, D., & Tyburczy, J. A. (2006). A numerical model for steady-state temperature distributions in solid-medium high-pressure cell assemblies. *American Mineralogist*, *91*(2–3), 295–305. https://doi.org/10.2138/am.2006.1938

Holtz, F., Roux, J., Ohlhorst, S., Behrens, H., & Schulze, F. (1999). The effects of silica and water on the viscosity of hydrous quartzofeldspathic melts. *American Mineralogist*, *84*(1–2), 27–36. https://doi.org/10.2138/am-1999-1-203

Huang, D., Li, Y., & Murakami, M. (2024). Low viscosity of peridotite liquid: Implications for magma ocean dynamics. *Geophysical Research Letters*, *51*(7), e2023GL107608. https://doi.org/10.1029/2023gl107608

Huang, W.-L., & Wyllie, P. J. (1975). Melting reactions in the system $NaAlSi_3O_8$-$KAlSi_3O_8$-SiO_2 to 35 kilobars, dry and with excess water. *The Journal of Geology*, *83*(6), 737–748. https://doi.org/10.1086/628165

Jing, Z., & Karato, S. I. (2011). A new approach to the equation of state of silicate melts: An application of the theory of hard sphere mixtures. *Geochimica et Cosmochimica Acta*, *75*(22), 6780–6802. https://doi.org/10.1016/j.gca.2011.09.004

21699356, 2025, 5, Downloaded from https://agupubs.onlinelibrary.wiley.com/doi/10.1029/2024JB030527 by Yanbin Wang - Argonne National Laboratory , Wiley Online Library on [03/06/2025]. See the Terms and Conditions (https://onlinelibrary.wiley.com/terms-and-conditions) on Wiley Online Library for rules of use; OA articles are governed by the applicable Creative Commons License

Kahle, A., Winkler, B., & Hennion, B. (2003). Is Faxén's correction function applicable to viscosity measurements of silicate melts with the falling sphere method? *Journal of Non-Newtonian Fluid Mechanics*, *112*(2–3), 203–215. https://doi.org/10.1016/s0377-0257(03)00098-3

Kanzaki, M., Kurita, K., Fujii, T., Kato, T., Shimomura, O., & Akimoto, S. (1987). A new technique to measure the viscosity and density of silicate melts at high pressure. *High-Pressure Research in Mineral Physics*, *39*, 195–200. https://doi.org/10.1029/gm039p0195

Karki, B. B., Bohara, B., & Stixrude, L. P. (2011). First-principles study of diffusion and viscosity of anorthite ($CaAl_2Si_2O_8$) liquid at high pressure. *American Mineralogist*, *96*(5–6), 744–751. https://doi.org/10.2138/am.2011.3646

Kelsey, K. E., Stebbins, J. F., Mosenfelder, J. L., & Asimow, P. D. (2009). Simultaneous aluminum, silicon, and sodium coordination changes in 6 GPa sodium aluminosilicate glasses. *American Mineralogist*, *94*(8–9), 1205–1215. https://doi.org/10.2138/am.2009.3177

Kobsch, A., & Caracas, R. (2020). The critical point and the supercritical state of alkali feldspars: Implications for the behavior of the crust during impacts. *Journal of Geophysical Research: Planets*, *125*(9), e2020JE006412. https://doi.org/10.1029/2020je006412

Kushiro, I. (1978). Viscosity and structural changes of albite ($NaAlSi_3O_8$) melt at high pressures. *Earth and Planetary Science Letters*, *41*(1), 87–90. https://doi.org/10.1016/0012-821x(78)90044-4

Ladenburg, R. (1907). Über den Einfluß von Wänden auf die Bewegung einer Kugel in einer reibenden Flüssigkeit. *Annalen der Physik*, *328*(8), 447–458. https://doi.org/10.1002/andp.19073280806

Laurent, O., Guitreau, M., Bruand, E., & Moyen, J. F. (2024). At the dawn of continents: Archean tonalite-trondhjemite-granodiorite suites. *Elements*, *20*(3), 174–179. https://doi.org/10.2138/gselements.20.3.174

Lee, S. K., Cody, G. D., Fei, Y., & Mysen, B. O. (2006). The effect of Na/Si on the structure of sodium silicate and aluminosilicate glasses quenched from melts at high pressure: A multi-nuclear (Al-27, Na-23, O-17) 1D and 2D solid-state NMR study. *Chemical Geology*, *229*(1–3), 162–172. https://doi.org/10.1016/j.chemgeo.2006.01.018

Lee, S. K., Yi, Y. S., Cody, G. D., Mibe, K., Fei, Y., & Mysen, B. O. (2011). Effect of network polymerization on the pressure-induced structural changes in sodium aluminosilicate glasses and melts: ^{27}Al and ^{17}O solid-state NMR study. *Journal of Physical Chemistry C*, *116*(3), 2183–2191. https://doi.org/10.1021/jp206765s

Leinenweber, K. D., Tyburczy, J. A., Sharp, T. G., Soignard, E., Diedrich, T., Petuskey, W. B., et al. (2012). Cell assemblies for reproducible multi-anvil experiments (the COMPRES assemblies). *American Mineralogist*, *97*(2–3), 353–368. https://doi.org/10.2138/am.2012.3844

Lorentz, H. A. (1907). Ein allgemeiner Satz, die Bewegung einer reibenden Flüssigkeit betreffend, nebst einigen Anwendungen desselben. *Abhandlungen über Theoretische Physik*, *1*, 23.

Makhluf, A. R., Newton, R. C., & Manning, C. E. (2020). Experimental investigation of phase relations in the system $NaAlSi_3O_8$–H_2O at high temperatures and pressures: Liquidus relations, liquid–vapor mixing, and critical phenomena at deep crust–upper mantle conditions. *Contributions to Mineralogy and Petrology*, *175*(8), 1–20. https://doi.org/10.1007/s00410-020-01711-2

Malfait, W. J., Verel, R., Ardia, P., & Sanchez-Valle, C. (2012). Aluminum coordination in rhyolite and andesite glasses and melts: Effect of temperature, pressure, composition and water content. *Geochimica et Cosmochimica Acta*, *77*, 11–26. https://doi.org/10.1016/j.gca.2011.11.011

Maude, A. D. (1961). End effects in a falling-sphere viscometer. *Journal of Applied Physics*, *12*(6), 293–295. https://doi.org/10.1088/0508-3443/12/6/306

Mollo, S., & Hammer, J. (2017). Dynamic crystallization in magmas. *European Mineralogical Union Notes in Mineralogy*, *16*, 373–418. https://doi.org/10.1180/EMU-notes.16.12

Mookherjee, M., Mainprice, D., Maheshwari, K., Heinonen, O., Patel, D., & Hariharan, A. (2016). Pressure induced elastic softening in framework aluminosilicate-albite ($NaAlSi_3O_8$). *Scientific Reports*, *6*(1), 34815. https://doi.org/10.1038/srep34815

Mori, S., Ohtani, E., & Suzuki, A. (2000). Viscosity of the albite melt to 7 GPa at 2000 K. *Earth and Planetary Science Letters*, *175*(1–2), 87–92. https://doi.org/10.1016/s0012-821x(99)00284-8

Mouser, M. D., Dygert, N., Anzures, B. A., Grambling, N. L., Hrubiak, R., Kono, Y., et al. (2021). Experimental investigation of Mercury's magma ocean viscosity: Implications for the formation of Mercury's cumulate mantle, its subsequent dynamic evolution, and crustal petrogenesis. *Journal of Geophysical Research: Planets*, *126*(11), e2021JE006946. https://doi.org/10.1029/2021je006946

Moyen, J. F., Janoušek, V., Laurent, O., Bachmann, O., Jacob, J. B., Farina, F., et al. (2021). Crustal melting vs. fractionation of basaltic magmas: Part 1, granites and paradigms. *Lithos*, *402*, 106291. https://doi.org/10.1016/j.lithos.2021.106291

Moyen, J. F., & Martin, H. (2012). Forty years of TTG research. *Lithos*, *148*, 312–336. https://doi.org/10.1016/j.lithos.2012.06.010

Neilson, R. T., Spera, F. J., & Ghiorso, M. S. (2016). Thermodynamics, self-diffusion, and structure of liquid $NaAlSi_3O_8$ to 30 GPa by classical molecular dynamics simulations. *American Mineralogist*, *101*(9), 2029–2040. https://doi.org/10.2138/am-2016-5486

Ono, S. (2022). Equation of state determination for rhenium using first-principles molecular dynamics calculations and high-pressure experiments. *Advances in Condensed Matter Physics*, *2022*, 1–6. https://doi.org/10.1155/2022/7545777

Poe, B. T., McMillan, P. F., Rubie, D. C., Chakraborty, S., Yarger, J., & Diefenbacher, J. (1997). Silicon and oxygen self-diffusivities in silicate liquids measured to 15 gigapascals and 2800 Kelvin. *Science*, *276*(5316), 1245–1248. https://doi.org/10.1126/science.276.5316.1245

Poe, B. T., Romano, C., Liebske, C., Rubie, D. C., Terasaki, H., Suzuki, A., & Funakoshi, K. (2006). High-temperature viscosity measurements of hydrous albite liquid using in-situ falling-sphere viscometry at 2.5 GPa. *Chemical Geology*, *229*(1–3), 2–9. https://doi.org/10.1016/j.chemgeo.2006.01.010

Pommier, A., & Le-Trong, E. (2011). "SIGMELTS": A web portal for electrical conductivity calculations in geosciences. *Computers and Geosciences*, *37*(9), 1450–1459. https://doi.org/10.1016/j.cageo.2011.01.002

Sakamaki, T., Suzuki, A., Ohtani, E., Terasaki, H., Urakawa, S., Katayama, Y., et al. (2013). Ponded melt at the boundary between the lithosphere and asthenosphere. *Nature Geoscience*, *6*(12), 1041–1044. https://doi.org/10.1038/ngeo1982

Schulze, F., Behrens, H., Holtz, F., Roux, J., & Johannes, W. (1996). The influence of H_2O on the viscosity of a haplogranitic melt. *American Mineralogist*, *81*(9–10), 1155–1165. https://doi.org/10.2138/am-1996-9-1014

Schulze, M., & Spiekermann, G. (2023). Fivefold-coordinated silicon in $MgSiO_3$ melt accommodates viscous flow up to transition zone pressures. *Geophysical Research Letters*, *50*(22), e2023GL105750. https://doi.org/10.1029/2023gl105750

Shimada, M. (1972). Melting of albite at high pressures under conditions. *Journal of Physical Earth*, *20*(1), 59–70. https://doi.org/10.4294/jpe1952.20.59

Skjerlie, K. P., & Johnston, A. D. (1993). Fluid-absent melting behavior of an F-rich tonalitic gneiss at mid-crustal pressures: Implications for the generation of anorogenic granites. *Journal of Petrology*, *34*(4), 785–815. https://doi.org/10.1093/petrology/34.4.785

Spice, H., Sanloup, C., Cochain, B., De Grouchy, C., & Kono, Y. (2015). Viscosity of liquid fayalite up to 9 GPa. *Geochimica et Cosmochimica Acta*, *148*, 219–227. https://doi.org/10.1016/j.gca.2014.09.022

Stewart, D. B., & Limbach, D. (1967). Thermal expansion of low and high albite. *American Mineralogist*, *52*, 389–413.

Stolper, E., Walker, D., Hager, B. H., & Hays, J. F. (1981). Melt segregation from partially molten source regions: The importance of melt density and source region size. *Journal of Geophysical Research*, *86*(B7), 6261–6271. https://doi.org/10.1029/jb086ib07p06261

21699356, 2025, 5, Downloaded from https://agupubs.onlinelibrary.wiley.com/doi/10.1029/2024JB030527 by Yanbin Wang - Argonne National Laboratory , Wiley Online Library on [03/06/2025]. See the Terms and Conditions (https://onlinelibrary.wiley.com/terms-and-conditions) on Wiley Online Library for rules of use; OA articles are governed by the applicable Creative Commons License

Sutterby, J. L. (1973). Falling sphere Viscometry - 1. Wall and inertial corrections to Stokes' law in long tubes. *Transactions of the Society of Rheology*, *17*(4), 559–573. https://doi.org/10.1122/1.549308

Suzuki, A., Ohtani, E., Funakoshi, K., Terasaki, H., & Kubo, T. (2002). Viscosity of albite melt at high pressure and high temperature. *Physics and Chemistry of Minerals*, *29*, 159–165.

Suzuki, A., Ohtani, E., Terasaki, H., Nishida, K., Hayashi, H., Sakamaki, T., et al. (2011). Pressure and temperature dependence of the viscosity of a $NaAlSi_2O_6$ melt. *Physics and Chemistry of Minerals*, *38*(1), 59–64. https://doi.org/10.1007/s00269-010-0381-4

Syracuse, E. M., van Keken, P. E., & Abers, G. A. (2010). The global range of subduction zone thermal models. *Physics of the Earth and Planetary Interiors*, *183*(1–2), 73–90. https://doi.org/10.1016/j.pepi.2010.02.004

Tange, Y., Nishihara, Y., & Tsuchiya, T. (2009). Unified analyses for P-V-T equation of state of MgO: A solution for pressure-scale problems in high P-T experiments. *Journal of Geophysical Research*, *114*(B3), 1–16. https://doi.org/10.1029/2008jb005813

Tenner, T. J., Lange, R. A., & Downs, R. T. (2007). The albite fusion curve re-examined: New experiments and the high-pressure density and compressibility of high albite and $NaAlSi_3O_8$ liquid. *American Mineralogist*, *92*(10), 1573–1585. https://doi.org/10.2138/am.2007.2464

Tinker, D., Lesher, C. E., Baxter, G. M., Uchida, T., & Wang, Y. (2004). High-pressure viscometry of polymerized silicate melts and limitations of the Eyring equation. *American Mineralogist*, *89*(11–12), 1701–1708. https://doi.org/10.2138/am-2004-11-1216

Urbain, G., Bottinga, Y., & Richet, P. (1982). Viscosity of liquid silica, silicates and aluminosilicates. *Geochimica et Cosmochimica Acta*, *46*(6), 1061–1072. https://doi.org/10.1016/0016-7037(82)90059-x

Wang, Y., Rivers, M., Sutton, S., Nishiyama, N., Uchida, T., & Sanehira, T. (2009). The large-volume high-pressure facility at GSECARS: A "Swiss-army-knife" approach to synchrotron-based experimental studies. *Physics of the Earth and Planetary Interiors*, *174*(1–4), 270–281. https://doi.org/10.1016/j.pepi.2008.06.017

Wang, Y., Sakamaki, T., Skinner, L. B., Jing, Z., Yu, T., Kono, Y., et al. (2014). Atomistic insight into viscosity and density of silicate melts under pressure. *Nature Communications*, *5*(1), 3241. https://doi.org/10.1038/ncomms4241

Williams, D. W., & Kennedy, G. C. (1970). The melting of jadeite to 60 kilobars. *American Journal of Science*, *269*(5), 481–488. https://doi.org/10.2475/ajs.269.5.481

Xie, L., Yoneda, A., Katsura, T., Andrault, D., Tange, Y., & Higo, Y. (2021). Direct viscosity measurement of peridotite melt to lower-mantle conditions: A further support for a fractional magma-ocean solidification at the top of the lower mantle. *Geophysical Research Letters*, *48*(19), e2021GL094507. https://doi.org/10.1029/2021gl094507

Xie, L., Yoneda, A., Yamazaki, D., Manthilake, G., Higo, Y., Tange, Y., et al. (2020). Formation of bridgmanite-enriched layer at the top lower-mantle during magma ocean solidification. *Nature Communications*, *11*, 1–10. https://doi.org/10.1038/s41467-019-14071-8

Yang, L., Karandikar, A., & Boehler, R. (2012). Flash heating in the diamond cell: Melting curve of rhenium. *Review of Scientific Instruments*, *83*(6), 2–7. https://doi.org/10.1063/1.4730595

Zhou, W. Y., Hao, M., Hrubiak, R., Kenney-Benson, C., & Zhang, J. S. (2024). Migration and accumulation of hydrous mantle incipient melt in the Earth's asthenosphere: Constraints from in-situ falling sphere viscometry measurements. *Earth and Planetary Science Letters*, *641*, 118833. https://doi.org/10.1016/j.epsl.2024.118833

References From the Supporting Information

Bouhifd, M. A., Whittington, A. G., & Richet, P. (2015). Densities and volumes of hydrous silicate melts: New measurements and predictions. *Chemical Geology*, *418*, 40–50. https://doi.org/10.1016/j.chemgeo.2015.01.012

Curetti, N., Sochalski-Kolbus, L. M., Angel, R. J., Benna, P., Nestola, F., & Bruno, E. (2011). High-pressure structural evolution and equation of state of analbite. *American Mineralogist*, *96*(2–3), 383–392. https://doi.org/10.2138/am.2011.3604

Dziewonski, A. M., & Anderson, D. L. (1981). Preliminary reference Earth model. *Physics of the Earth and Planetary Interiors*, *25*(4), 297–356. https://doi.org/10.1016/0031-9201(81)90046-7

Kress, V. C., Williams, Q., & Carmichael, I. S. E. (1988). Ultrasonic investigation of melts in the system Na_2O-Al_2O_3-SiO_2. *Geochimica et Cosmochimica Acta*, *52*(2), 283–293. https://doi.org/10.1016/0016-7037(88)90084-1

Lange, R. A. (1997). A revised model for the density and thermal expansivity of K_2O-Na_2O-CaO-MgO-Al_2O_3-SiO_2 liquids from 700 to 1900 K: Extension to crustal magmatic temperatures. *Contributions to Mineralogy and Petrology*, *130*, 1–11. https://doi.org/10.1007/s004100050345

Lange, R. A., & Carmichael, I. S. E. (1987). Densities of Na_2O-K_2O-CaO-MgO-FeO-Fe_2O_3-Al_2O_3-TiO_2-SiO_2 liquids: New measurements and derived partial molar properties. *Geochimica et Cosmochimica Acta*, *51*(11), 2931–2946. https://doi.org/10.1016/0016-7037(87)90368-1

Ni, H., & Zhang, Y. (2008). H_2O diffusion models in rhyolitic melt with new high-pressure data. *Chemical Geology*, *250*(1–4), 68–78. https://doi.org/10.1016/j.chemgeo.2008.02.011

Ochs, F. A., & Lange, R. A. (1997). The partial molar volume, thermal expansivity and compressibility of H_2O in $NaAlSi_3O_8$ liquid: New measurements and an internally consistent model. *Contributions to Mineralogy and Petrology*, *129*(2–3), 155–165. https://doi.org/10.1007/s004100050329

Wang, J., Mao, Z., Jiang, F., & Duffy, T. S. (2015). Elasticity of single-crystal quartz to 10 GPa. *Physics and Chemistry of Minerals*, *42*(3), 203–212. https://doi.org/10.1007/s00269-014-0711-z

Zhao, Y., Von Dreele, R. B., Shankland, T. J., Weidner, D. J., Zhang, J., Wang, Y., & Gasparik, T. (1997). Thermoelastic equation of state of jadeite $NaAlSi_2O_6$: An energy-dispersive Rietveld refinement study of low symmetry and multiple phases diffraction. *Geophysical Research Letters*, *24*(1), 5–8. https://doi.org/10.1029/96gl03769

21699356, 2025, 5, Downloaded from https://agupubs.onlinelibrary.wiley.com/doi/10.1029/2024JB030527 by Yanbin Wang - Argonne National Laboratory , Wiley Online Library on [03/06/2025]. See the Terms and Conditions (https://onlinelibrary.wiley.com/terms-and-conditions) on Wiley Online Library for rules of use; OA articles are governed by the applicable Creative Commons License